Multiple signaling pathways converge onto the regulation of HAD-like phosphatases to modulate cellular resistance to the metabolic inhibitor, 2-deoxyglucose

Quentin Defenouillère[1,2], Agathe Verraes[1,2], Clotilde Laussel[1], Anne Friedrich[3], Joseph Schacherer[3] & Sébastien Léon[1,4]

1: Institut Jacques Monod, UMR 7592 Centre National de la Recherche Scientifique/Université Paris-Diderot, Sorbonne Paris Cité, Paris, France

2: These authors contributed equally to this work

3: Université de Strasbourg, CNRS, GMGM UMR 7156, Strasbourg, France

4: Author for correspondence:

Sébastien Léon, PhD

Institut Jacques Monod

15 Rue Hélène Brion

75205 Paris Cedex 13, France.

email: sebastien.leon@ijm.fr; tel. +33 (0)1 57 27 80 57.

Abstract

Cancer cells display an altered metabolism with an increased glycolysis and a lower respiration rate, leading to an increased glucose uptake. These particularities provide therapeutic opportunities and anti-cancer strategies targeting glycolysis through metabolic inhibitors have been put forth. One of these inhibitors, the glucose analogue 2-deoxyglucose (2DG), is imported into cells and phosphorylated into 2DG-6-phosphate, a toxic by-product that accumulates in cells and inhibits glycolysis. Recent data suggest that 2DG has additional effects in the cell, and resistance to 2DG has also been observed. It appears crucial to better understand the mechanisms leading to this resistance. Using budding yeast as a model system, we engaged an unbiased, mass-spectrometry-based approach to probe the cellular effects of 2DG exposure on the total proteome and reveal the molecular basis of 2DG resistance. This led to the identification of two 2DG-6-Phosphate phosphatases, Dog1 and Dog2, that are induced upon exposure to 2DG and participate in 2DG detoxification. We reveal that 2DG induces Dog2 by upregulating several signaling pathways, such as the MAPK (Hog1/p38)-based stress-responsive pathway, the Unfolded Protein Response (UPR) pathway triggered by 2DG-induced ER stress, and the MAPK (Slt2)-based Cell Wall Integrity pathway. Consequently, loss of the UPR or CWI pathways leads to hypersensitivity to 2DG. Moreover, we show that *DOG2* is additionally regulated by glucose availability in a Snf1/AMPK-dependent manner through the transcriptional repressors Mig1/Mig2 and Cyc8, explaining why several mutants impaired in this pathway were found as 2DG-resistant. The isolation and characterization of spontaneous 2DG-resistant mutants revealed that *DOG2* overexpression is a common strategy for 2DG resistance. Thus, 2DG-induced interference with cellular signaling rewires the expression of these endogenous phosphatases to promote 2DG resistance. Importantly, a human orthologue of Dog1/Dog2, named HDHD1, displays an *in vitro* 2DG-6-phosphate phosphatase activity, and its overexpression confers 2DG resistance in HeLa cells, which has important implications for potential future chemotherapies involving 2DG.

Introduction

Most cancer cells display an altered metabolism, with an increased glucose consumption to support their proliferative metabolism that is based on aerobic glycolysis (Warburg effect) (1, 2). Targeting glycolysis has been proposed as a strategy to target cancer cells and various metabolic inhibitors have been considered (3, 4).

2-deoxy-D-glucose (2DG) is a derivative of D-glucose that is actively imported by glucose transporters and is phosphorylated by hexokinase into 2-deoxy-D-glucose-6-phosphate (2DG6P), but cannot be further metabolized due to the 2-deoxy substitution, triggering a decrease in cellular ATP content in tumors (5). Mechanistically, 2DG6P accumulation hampers glycolysis by inhibiting hexokinase activity in a non-competitive manner (6, 7), as well as phospho-glucose isomerase activity in a competitive manner (8). Since cancer cells rely on an increased glycolysis rate for proliferation, 2DG has been of interest for cancer therapy, particularly in combination with radiotherapy or other metabolic inhibitors (9-11). These features led to a phase I clinical trial using 2DG in combination with other drugs to treat solid tumors (12). Its derivative ^{18}Fluoro-2DG is also used in cancer imaging (PET scans) as it preferentially accumulates in tumor cells due to their increased glucose uptake (13). Additionally, due to its structural similarity to mannose, 2DG (which could also be referred as to 2-deoxymannose, since mannose is the C2 epimer of glucose) also interferes with N-linked glycosylation and causes ER stress (14-16) and this was proposed to be the main mechanism by which 2DG kills normoxic cells (17). Recently, 2DG toxicity was also linked to the depletion of phosphate pools following 2DG phosphorylation (18). Finally, interference of 2DG with lipid metabolism and calcium homeostasis was also described, but the underlying mechanisms are less clear (19). Intriguingly, despite its pleiotropic mode of action, resistance to 2-deoxyglucose was reported in cell cultures (20).

Because these metabolic and signalling pathways are evolutionarily conserved, simpler eukaryotic models such as the budding yeast *Saccharomyces cerevisiae* can be used to understand the mode of action of 2DG. Moreover, yeast is particularly well-suited for these studies because of its Warburg-like metabolism (21). Akin to cancer cells, *Saccharomyces cerevisiae* privileges glucose

consumption through glycolysis over respiration, regardless of the presence of oxygen. This is allowed by a glucose-mediated repression of genes involved in respiration and alternative carbon metabolism, which operates at the transcriptional level. This glucose-mediated repression mechanism is relieved upon activation of the yeast orthologue of AMPK, Snf1, which phosphorylates the transcriptional repressor Mig1 and leads to its translocation out of the nucleus (22-25). Previous studies in yeast identified mutations that render yeast cells more tolerant to 2DG (26-31). This suggested the existence of cellular mechanisms that can modulate 2DG toxicity, which are important to characterize if 2DG were to be used for therapies.

In yeast, 2DG was initially used to identify genes involved in glucose repression. This was based on the observation that 2DG, like glucose, causes Snf1 inactivation and thus prevents the use of alternative carbon sources (32-34). The characterization of mutants that were able to grow in sucrose medium despite the presence of 2DG allowed the identification of actors of the glucose repression pathway (26, 29, 35). These experiments also revealed that mutations in *HXK2,* encoding hexokinase II, also rendered yeast cells more tolerant to 2DG, perhaps by limiting 2DG phosphorylation and 2DG6P accumulation (29-31, 36, 37). Finally, several 2DG-resistant mutants displayed an increased 2DG6P phosphatase activity, which could detoxify the cells of this metabolite and dampen its negative effects on cellular physiology (38, 39). Indeed, two 2DG6P phosphatases were subsequently cloned, named *DOG1* and *DOG2,* and their overexpression led to 2DG resistance and prevented the 2DG-mediated repression of genes (33, 40, 41).

More recently, the toxicity of 2DG was studied in the context of glucose-grown cells, which may be more relevant for the understanding its mode of action in mammalian cells. In these conditions, 2DG toxicity is independent of its effect on the glucose repression of genes, but involves distinct mechanisms, such as a direct inhibition of glycolysis and other cellular pathways (30, 42, 43). Accordingly, several mutations initially identified as leading to 2DG tolerance in sucrose medium have no effect in glucose medium (30, 44). A key finding was that the deletion of *REG1*, encoding a regulatory subunit of Protein Phosphatase 1 (PP1) that negatively regulates Snf1 (45, 46) leads to 2DG

resistance (30). The resistance of the *reg1Δ* mutant depends on the presence of Snf1, and the single deletion of *SNF1* also renders yeast hypersensitive to 2DG (31). These data demonstrate that Snf1 activity is crucial for 2DG resistance. A model was proposed in which the 2DG sensitivity displayed by the *snf1*Δ mutant involves a misregulated expression and localization of the low-affinity glucose transporters, Hxt1 and Hxt3 (47). Additionally, the deletion of *LSM6*, which encodes a component of a complex involved in mRNA degradation, also leads to 2DG resistance in a Snf1-dependent manner, but the mechanism by which this occurs is unknown (31). Thus, many aspects of the pathways mediating 2DG sensitivity/resistance remain to be explored.

In the present study, we engaged an unbiased, mass-spectrometry-based approach in yeast to better understand the cellular response to 2DG. This revealed that the main 2DG6P phosphatase, Dog2, is induced upon exposure to 2DG and participates in 2DG detoxification in glucose medium. We reveal that 2DG induces Dog2 (and Dog1, to a certain extent), by upregulating several stress-responsive signaling pathways (UPR and MAPK-based pathways). Moreover, the expression of *DOG2* is additionally regulated by Snf1 and the glucose-repression pathway through the action of downstream transcriptional repressors, and contributes to the resistance of glucose-repression mutants to 2DG. The partial characterization of 24 spontaneous 2DG-resistant mutants revealed that most display an increased *DOG2* expression, suggesting it is a common strategy used to acquire 2DG resistance. Particularly, genome resequencing identified that mutations in *CYC8*, encoding a transcriptional corepressor, cause 2DG resistance through the upregulation of Dog2. The identification of a potential human orthologue of the Dog1/2 proteins, named HDHD1, which displays an *in vitro* 2-DG-6-phosphate phosphatase activity and which can cause resistance of HeLa cells to 2DG when overexpressed, suggests that HAD-like phosphatases are conserved regulators of 2DG resistance.

Results.

A proteomic assessment of the cellular response to 2DG reveals an increased expression of metabolic enzymes

As a first step to characterize the cellular response of yeast cells to 2-deoxyglucose (2DG) treatment in an unbiased and quantitative manner, we performed proteome-wide mass spectrometry-based proteomics on wild-type cells treated for 2.5 hours with 0.2% 2DG, a concentration that prevents growth of WT cells on plates (30) using untreated cells as a negative control. Overall, 78 proteins were significantly up-regulated, whereas 18 proteins were down-regulated after 2DG treatment (False Discovery Rate of 0.01) (**Figure 1A, Figure S1A, Table S1**). Among the up-regulated candidates, a significant enrichment of proteins involved in various metabolic processes was noted, including that of glucose, glucose-6-phosphate and other carbohydrates (**Figure S1B**).

Interestingly, these proteomics data revealed an increase in the abundance of the 2-deoxyglucose-6-phosphate phosphatases Dog1 or Dog2, which could not be discriminated at the mass spectrometry level because of their high sequence identity (92%). Dog1 and Dog2 were thus individually GFP-tagged at their chromosomal locus, in order to maintain an endogenous regulation, and their expression was monitored by western blotting. This revealed that both Dog1 and Dog2 expression levels are increased in the presence of 2DG, and that Dog2-GFP is more abundant than Dog1-GFP (**Figure 1B**).

To evaluate the contribution of transcription in the regulation of the *DOG1* and *DOG2* genes by 2DG, the corresponding promoters (1kb) were fused to a beta-galactosidase reporter. This revealed an increased activity of the *DOG1* and *DOG2* promoters in response to 2DG (**Figure 1C**), suggesting that the expression of Dog1 and Dog2 is, at least in part, due to an increased transcription. Of note, the deletion of the *DOG2* gene strongly sensitized yeast cells to 2-deoxyglucose, but that of *DOG1* had little effect (**Figure 1D**), indicating that Dog2 is functionally more important than Dog1, perhaps due to its higher expression level (**Figure 1B**).

The increased expression of Dog1 and Dog2 in response to 2DG was intriguing because it raised the question of how exposure to this synthetic molecule could trigger an adaptive resistance mechanism

in yeast. Prior work showed that the expression of Dog2, whose endogenous function in regular yeast metabolism is unknown, is induced by various stresses, such as oxidative and osmotic stresses, through the stress-responsive MAP kinase orthologue of p38, Hog1 (48). To determine whether this mechanism takes part in Dog1/2 regulation by 2DG, we first tested the effect of 2DG on Hog1 phosphorylation using an antibody directed against the phosphorylated form of mammalian p38 (49). Hog1 was activated upon 2DG addition, but to a much lower extent as by inducing hyperosmotic shock (**Figure 1E**). The deletion of *HOG1* indeed caused a partial decrease in Dog2 induction (**Figure 1F-H**), but had no discernable effect on the expression of Dog1. Altogether, we conclude that the stress-activated protein kinase Hog1 has no effect on Dog1 induction by 2DG treatment, and only participates in the induction of Dog2. This suggests that upregulation of Dog1 and Dog2 by 2DG involves at least one additional level of regulation.

The expression of Dog1 and Dog2 is induced by the Unfolded Protein Response pathway through 2-deoxyglucose-induced ER stress

Exposure of cancer cells to 2-deoxyglucose interferes with N-linked glycosylation, likely because of the structural similarity of 2-deoxyglucose with mannose, a constituent of the N-glycan structures (14). This results in endoplasmic reticulum (ER) stress and consequently, in the induction of the Unfolded Protein response (UPR) in mammalian cells (14). Accordingly, the glucose fluorescent analogue 2-NBDG ((2-(*N*-(7-Nitrobenz-2-oxa-1,3-diazol-4-yl)Amino)-2-Deoxyglucose), which was previously used in yeast as a glucose tracer (50) and which, much like 2DG, cannot be fully metabolized because of the lack of a hydroxyl group in position 2, partially co-localized with an ER marker (**Figure 2A**), suggesting interference with N-glycosylation which takes place at this organelle. Treatment of yeast with 2DG also induced a defect in the glycosylation of carboxypeptidase Y (CPY), a vacuolar (lysosomal) protease whose membrane-anchored precursor is N-glycosylated in the course of its intracellular trafficking (51). This defect was not as extensive as that observed upon treatment of cells with tunicamycin, an inhibitor of the first step of glycosylation that also causes ER stress and is a strong UPR inducer (52, 53)

(Figure 2B). Interestingly, the addition of exogenous mannose in the medium suppressed the glycosylation defects caused by 2DG, but not those caused by tunicamycin (Figure 2B). This supports the idea that 2DG mimics mannose and interferes with its incorporation in N-glycans, as proposed in mammalian cells (14, 17). 2DG treatment also led to the induction of an UPR element-containing reporter, UPRE1-LacZ (53) (Figure 2C). This depended on Hac1, a transcription factor whose regulated splicing occurs in response to ER stress and triggers the onset of the UPR response (53), confirming that 2DG is a *bona fide* UPR inducer (Figure 2C).

We then tested whether this induction of the UPR pathway contributes to the 2DG-mediated induction of Dog2. First, we found that tunicamycin strongly induced the *pDOG2*-LacZ reporter (Figure 2D). Moreover, the induction of this reporter by 2DG was reduced by more than 2-fold in a *hac1Δ* mutant, suggesting a contribution of the UPR in this induction (Figure 2E). Comparable results were obtained for p*DOG1*-LacZ (Figure S3). These results were confirmed at the protein level for Dog2 (Figure 2F-G).

Interestingly, UPR-compromised mutants such as *hac1*Δ and *ire1*Δ are both hypersensitive to 2DG (Figure 2H), suggesting that they cannot cope with ER stress caused by 2DG. However, the addition of exogenous mannose in the medium restored 2DG-tolerance of these mutants to a comparable level as the WT (Figure 2H). Altogether, these results confirm that 2DG induces ER stress by interfering with N-glycosylation, that the subsequent activation of the UPR pathway upregulates Dog1 and Dog2 expression and that UPR mutants display a lower level of Dog1 and Dog2 expression. Noticeably, Dog2 overexpression restored the growth of *hac1*Δ or *ire1*Δ cells at various concentrations of 2DG (Figure 2I).

2DG also activates the MAPK-based cell-wall integrity pathway which additionally contributes to Dog1 and Dog2 expression

To address a possible additional contribution of other signaling pathways that would contribute to the 2-DG-induced expression of Dog1 and Dog2, we ran a bioinformatics analysis on the list of proteins

that were found as upregulated upon 2DG treatment (see **Figure 1A**, and **Table S1**) using YEASTRACT (54) to evaluate whether the observed variations in protein expression could reveal a potential transcriptional signature. The best hit (corresponding to 35/78 candidates, *p*-value=0) was the MADS-box transcription factor Rlm1, a known downstream target of the cell wall integrity (CWI) pathway (55). There are well-established links between CWI signaling and ER stress (56-60), and indeed, 2DG treatment induced the phosphorylation of the CWI MAPK, Slt2, within the first hour of exposure (**Figure 3A**). Accordingly, 2DG led to the transcriptional induction of an Rlm1-regulated promoter fused to LacZ (**Figure 3B**). Importantly, the deletion of many genes of the cell-wall integrity pathway acting upstream of Rlm1 caused an increased 2DG sensitivity (**Figure 3C**) such as those encoding the sensors *MID2* and *WSC1*. Thus, much like the UPR pathway, the CWI pathway is required for 2DG tolerance.

We thus questioned whether CWI pathway activation by 2DG contributed to Dog1 and Dog2 induction. Indeed, the activity of both promoters was decreased in the *slt2*Δ mutant (**Figure 3D** and **S4**). This was confirmed for Dog2 by analyzing the expression levels of Dog2-GFP (**Figure 3E-F**). Thus, similarly to tunicamycin (58), 2DG acts as an inducer of cell-wall integrity signaling and participates in Dog1 and Dog2 induction, in addition to the UPR pathway. Interestingly, however, the addition of exogenous mannose did not lead to a better tolerance of CWI mutants to 2DG (**Figure 3G**). Thus, ER stress relief is not sufficient to suppress 2DG toxicity in these mutants, suggesting that 2DG has other effects in the cell beyond triggering ER stress.

A third pathway negatively regulates the expression of Dog2, but not Dog1, by glucose availability and participates in the described resistance of glucose-repression mutants to 2DG

The toxicity of 2DG also lies in the fact that it impairs glycolysis by inhibiting hexokinase and phosphoglucose isomerase activity (6-8). This leads to an energetic stress and accordingly, 2DG treatment activates AMPK in mammals (61).

Several lines of evidence indicate that the activity of the yeast AMPK orthologue, Snf1, is important for 2DG tolerance. Whereas the *snf1*Δ mutant is hypersensitive to 2DG, the *reg1*Δ mutant, in which

Snf1 is hyperactive, displays an increased resistance towards 2DG which depends on Snf1 activity (31). A previous study showed that Snf1 positively regulates Dog2 expression (48), so we hypothesized that the *snf1Δ* mutant may be hypersensitive to 2DG because of a lack of Dog2 expression. To first confirm the effect of Snf1 on Dog1 and Dog2 expression, glucose-grown cells were transferred to a medium containing lactate as a sole carbon source, which is known to cause Snf1 activation and consequently, the de-repression of glucose-repressed genes. The expression of Dog2, was increased in this condition, but not that of Dog1 (**Figure 4A**). This occurred in a Snf1-dependent manner. In line with these data, the *pDOG2*-LacZ reporter was induced after transfer to lactate medium, but this response was decreased in the *snf1Δ* mutant, confirming that *DOG2* is subject to a glucose-repression mechanism and is thus constantly repressed in a *snf1Δ* mutant (**Figure 4B**), which may explain why the *snf1*Δ mutant is sensitive to 2DG. A previous report indicated that Dog1/2 overexpression in a *snf1Δ* mutant did not rescue resistance to 2DG, but we thought that this might be due to the fact that these experiments involved a high-copy plasmid in which Dog2 expression was still under the control of its endogenous, i.e. Snf1-regulated, promoter (47). Indeed, when overexpressed using a strong and constitutive promoter (*pGPD*), Dog2 could rescue Snf1 growth on 2DG (**Figure 4C**).

In contrast, Dog2 expression was increased in glucose-repression mutants which display an increased Snf1 activity, such as mutants lacking the hexokinase Hxk2 or the PP1 regulatory phosphatase Reg1 (44, 62), both at the promoter level and the protein level (**Figure 4D-E**). In addition, lack of the Snf1-regulated transcriptional repressors Mig1/Mig2 also led to an increase in Dog2 expression (**Figure 4D-E**). A regulatory sequence in the promoter, present between -250 and -350 bp relative to the ATG, combined with a proposed Mig1-binding site located at ca. -200 bp (40, 48) was critical for this glucose-mediated repression (**Figure S5**). Interestingly, mutants showing an increased Dog2 expression such as *reg1Δ* or *hxk2Δ* are known to be more tolerant to 2DG than the WT (30, 31), and we report that this is also the case for the double mutant *mig1Δ mig2Δ* (**Figure 4F**). We deleted *DOG1* and *DOG2* in these mutants to evaluate their contribution to 2DG resistance. The absence of Dog1 and Dog2 sensitized all strains to 2DG (**Figure 4F**); in particular, the *mig1Δ mig2Δ dog1Δ dog2Δ*

regained a sensitivity comparable to that of the WT, demonstrating that the resistance displayed by the *mig1Δ mig2Δ* mutant is due to an increased *DOG* expression. In contrast, the *reg1Δ dog1Δ dog2Δ* and the *hxk2Δ dog1Δ dog2Δ* strains still remained more resistant than the WT, suggesting additional mechanisms of resistance. Finally, we observed that the *snf1Δ mig1Δ mig2Δ* was resistant to 2DG despite the absence of Snf1, in line with the idea that the *snf1Δ* is 2DG-sensitive because of the constitutive repression of Mig1/Mig2 target genes, such as Dog1 and Dog2 and possibly other genes (Figure 4F). Overall, we conclude that Dog2 presents an additional regulation by glucose availability through Snf1/AMPK activity, which participates in the well-described resistance of glucose-repression mutants to 2DG.

Increased expression of *DOG2* is frequently observed in spontaneous 2DG-resistant clones

Previous screens led to the identification of 2DG-resistant mutants (26, 29, 35). The initial purpose of these screens was to identify mutants that were insensitive to the repressive effect of 2DG, or that were impaired for glucose phosphorylation (since only 2DG6P is toxic to cells), and consequently, were performed on media containing other carbon sources than glucose.

The mechanisms involved in 2DG resistance on glucose medium were tackled much later by screening of the deletion library (30), which led to the identification of resistant mutants, some of which were subsequently confirmed (31). In the course of our experiments, we often found that 2DG-resistant clones could spontaneously arise from wild-type or even 2DG-susceptible strains (see examples in the drop tests of Figure 1D or 2H). Indeed, it was previously noted that yeast acquires 2DG resistance at a high frequency, which can be accompanied by an increase in 2DG-6-phosphatase activity (28, 38). To study whether Dog2, which is functionally the most important paralogue for 2DG resistance, is upregulated during the emergence of spontaneous 2DG-resistant mutants, we spread ca. $2x10^6$ cells on a glucose-based medium containing 0.2% 2DG, and selected clones that had appeared after 6 days of growth. Altogether, 24 clones were obtained, whose resistance to 2DG was confirmed (see Figure 5B). Using the p*DOG2*-LacZ reporter, we found that 13 clones displayed a significantly

increased *DOG2* promoter activity as compared to WT strains (**Figure 5A**). This suggested that Dog2 overexpression is a frequent feature of 2DG-resistant clones. Among those, we expected to isolate *reg1* and *hxk2* mutants because both are resistant to 2DG in glucose medium (See Figure 4F; 30, 31). To identify them, we first tested whether some of the isolated resistant clones displayed phenotypes typical of *reg1* mutants, such as sensitivity to tunicamycin (63, 64) or selenite (which enters the cell through the glucose-repressed transporter Jen1: 65, 66), which allowed to discriminate potential *reg1* mutants from *hxk2* mutants (**Figure 5B**). Indeed, three of the isolated clones were potential *reg1* mutants based on these phenotypes (**Figure 5A**). This was further supported by the observation that these 3 mutants displayed a markedly increased activation of Snf1, as measured by using an antibody directed against phosphorylated AMPK (**Figure 5C**). Sequencing of the *REG1* coding sequence in these clones revealed point mutations (substitutions) causing the appearance of stop codons which likely explain Reg1 loss of function (**Figure 5D**). To additionally identify whether the set of spontaneous resistant clones contained *hxk2* mutants, we performed a complementation test and therefore crossed these strains with either a WT strain or an *hxk2Δ* strain and tested the ability of the resulting diploids to grow on 2DG. All diploids generated through the cross with the WT lost their ability to grow on 2DG, except two (clones #23 and #24) (**Figure 5E**), indicating that 2DG resistance was generally caused by (a) recessive mutation(s). In contrast, 12 diploids obtained by the cross with the *hxk2Δ* strain maintained their ability to grow on 2DG (**Figure 5E**), suggesting that 2DG resistance of the initial strains was caused by a deficiency in *HXK2* function. Most of these clones also displayed an increased p*DOG2*-LacZ expression, in agreement with our previous findings (**Figure 4D-E**). We PCR-amplified and sequenced the *HXK2* ORF in the WT and these mutants (**Figure 5F**). Out of the 12 mutants identified that are in the same complementation group as *HXK2*, two did not display any mutation in the *HXK2* ORF (clones #1 and #8) and may represent regulatory mutants in *cis*, possibly in regions that were not sequenced. In favor of this hypothesis, we found that their 2DG sensitivity can be restored by re-expression of *HXK2* using a multicopy, genomic clone (**Figure S6A**). The other 10 mutants carried at least one mutation in the *HXK2* coding sequence (**Figure 5F**). Four mutations created a stop codon

(clones #12, #15, #16 and #20) resulting in a predicted protein that was truncated almost fully (#20: mutation Leu^{4}>TAA) or by more than half of its length, which is expected to lead to loss of function since conserved regions present in the C-terminal domain are essential for ATP binding and hexokinase activity (67, 68). Five mutants (#2, #3, #11, #13 and #14) carried a single point mutation in residues conserved across all hexokinase sequences tested (see alignment, **Figure S6, B-C**). Four of these affected residues in close proximity to glucose binding residues (#2: T^{212}>P; #3: K^{176}>T; #11 and #14: Q^{299}>H) (69). The fifth mutation (#13: G^{418}>C) was located next to S^{419}, proposed to interact with the adenosine moiety of ATP (67, 69). Finally, one mutant (#21) bared two mutations, T^{75}>I and S^{345}>P, the latter of which introduces a Pro residue nearby a putative ADP-binding pocket (69, 70). However, these residues are much less conserved (**Figure S6C**) so it could be that both mutations combined are required to abolish Hxk2 function, although this is only speculative.

Among the 2DG-resistant clones which expressed *pDOG2*-LacZ at a high level, 2 clones (#9 and #10) remained unaccounted for by mutations in either *REG1* or *HXK2*, suggesting that their resistance involved a novel mechanism. Whole genome resequencing of the genomic DNA isolated from these clones and comparison with that of the parent strain revealed several SNPs (**Table S2**) including a nonsense mutation in *CYC8* (C^{958}>T) that was identified in both strains, causing a premature stop codon at position 320 (**Figure 6A**). The *CYC8* gene is also known as *SSN6* (*Suppressor of snf1*) and mutations in this gene lead to constitutive expression of the glucose-repressed gene encoding invertase (*SUC2*), even in a *snf1* mutant (71, 72). Indeed, *CYC8* encodes a transcriptional co-repressor which controls the expression of glucose-regulated genes (73). Because the repression of *DOG2* expression by glucose is controlled by Snf1 and Mig1/Mig2 (see **Figure 4**), we hypothesized that *CYC8* could also take part in *DOG2* regulation, so that a mutation in *CYC8* could lead to increased 2DG resistance through *DOG2* overexpression. We observed that indeed, mutants #9 and #10 expressed invertase even in when grown in glucose medium (repressive conditions), in agreement with a mutation in *CYC8* (**Figure 6B**). We also observed that these mutants displayed an increased adhesion phenotype, i.e. persistence of colony structures upon washing the plate (74) that is often associated to mutants that are prone to

flocculate, such as *cyc8* mutants (75, 76) (Figure 6C). When we introduced a low copy (centromeric) plasmid containing *CYC8* under the control of its endogenous promoter, we observed that it suppressed the 2DG resistance of mutants #9 and #10 as well as their adhesion to the agar plate (Figure 6C). This was not the case when using a truncated version of *CYC8* identified in this screen (Figure 6C), although mutants #9 and and #10 did not display a slow growth contrary to the *cyc8Δ* mutant, suggesting that it is at least partially active for other functions. Finally, we tested whether the strong activity of the *DOG2* promoter observed in mutants #9 and #10 (see Figure 5A) was also due to the lack of a functional *CYC8*. Indeed, the re-introduction of low-copy vector containing *CYC8* led to a decreased reporter expression in these mutants (Figure 6D). This was confirmed by examining Dog2-GFP expression at the protein level (Figure 6E-F). Therefore, *DOG2* expression is regulated by Cyc8 and spontaneous *cyc8* mutants display an increase in Dog2 expression and increased resistance to 2DG.

Altogether, this initial characterization revealed that *DOG2* overexpression is a common phenomenon within spontaneous 2DG-resistant clones, both in known 2DG-resistant mutants (*reg1* and *hxk2*) and in the novel 2DG-resistant *cyc8* mutants that we isolated.

HDHD1, a human member of the HAD-like phosphatase family, is a new 2DG-6-P phosphatase involved in 2DG resistance

The fact that Dog2 expression is increased in various spontaneous 2DG-resistant mutants reminded us of early studies in HeLa cells showing an increased 2DG6P phosphatase activity in isolated 2DG resistant clones (20). Dog1 and Dog2 belong to the family of HAD (Haloacid Dehalogenase)-like phosphatases conserved from bacteria to human (Figure 7A). The bacterial homolog of Dog1/Dog2, named YniC, can also dephosphorylate 2DG6P *in vitro* (77) and we found that the expression of YniC in the double *dog1*Δ *dog2*Δ yeast mutant also restored 2DG resistance (Figure 7B). We used this phenotype to identify potential human orthologues (Figure 7A). Running a PSI-BLAST (78) on the human proteome using the Dog2 protein sequence retrieved HDHD1-isoform a (NP_036212.3) as the best hit (39% homology). HDHD1 (for Haloacid Dehalogenase-like Hydrolase Domain containing 1; also

named PUDP for pseudouridine-5'-phosphatase) is a HAD-like phosphatase with a demonstrated *in vitro* activity towards phosphorylated metabolites such as pseudouridine-5'-phosphate (79). When expressed in in the double *dog1*Δ *dog2*Δ mutant, HDHD1 was partially able to rescue growth on 2DG containing medium (**Figure 7B**). The expression of HDHD4 (also named NANP, for N-acylneuraminate-9-phosphatase; 80), which belongs to the same subfamily as HDHD1 within the HAD-phosphatase family (37% homology), did not significantly restore yeast growth on 2DG (**Figure 7C, D**), neither did that of PSPH (phosphoserine phosphatase; 81), another close family member (**Figure 7C**). Moreover, among the four predicted isoforms of HDHD1 (isoforms 1-4), only HDHD1-1 rescued the growth of the *dog1*Δ *dog2*Δ on 2DG-containing medium (**Figure 7E**) despite the fact that all isoforms were expressed in yeast, as confirmed by western blotting using anti-HDHD1 antibodies (**Figure 7F**).

The mutation of conserved aspartate residues (D^{12} and D^{14}, see alignment in **Figure 7A**), predicted to be essential for the catalytic activity of HAD phosphatases (82) abolished the ability of HDHD1 to restore growth of the *dog1*Δ *dog2*Δ mutant on 2DG (**Figure 8A, B**), suggesting it may act as a 2DG-6P phosphatase. This was confirmed by purifying recombinant HDHD1 (**Figure 8C**) and testing for a potential 2DG-6-P phosphatase activity. Indeed, HDHD1 could dephosphorylate 2DG-6P *in vitro*, and this activity depended on the integrity of its putative catalytic residues (**Figure 8D**). We then tested whether HDHD1 overexpression in HeLa cells could lead to an increased resistance to 2-DG. Low concentrations of 2DG (5 mM) in the presence of glucose (25 mM) were sufficient to inhibit the growth of cells transfected with an empty vector, whereas those that overexpressed HDHD1 were virtually insensitive to 2DG treatment (**Figure 8E**). Importantly, HDHD1 expression was not influenced by ER stress in HeLa cells, since exposure to 2DG or tunicamycin did not modify the expression level of endogenous HDHD1 (despite affecting the glycosylation of CD147, a heavily glycosylated plasma membrane protein) (**Figure 8F**). These results suggest that a dysregulated expression of HDHD1 could modulate 2DG resistance.

Discussion

The first studies examining the effect of 2DG on glycolysis in yeast but also in normal and cancer tissues were published more than 60 years ago (83-85). Yet, its mode of action is not fully understood. For a given concentration, 2DG inhibits yeast growth more potently in a medium containing 2% glucose than 5% glucose (86), thus 2DG can be considered as a general competitor of glucose. Because of its structural similarity to glucose and its described effect on the inhibition of glycolytic enzymes (6-8), 2DG was mostly considered as a glycolysis inhibitor, but more recent data challenged this view (87). Indeed, exposure of cancer cells to 2-deoxyglucose interferes with N-linked glycosylation, likely because of the structural similarity of 2-deoxyglucose with mannose. This results in endoplasmic reticulum (ER) stress and consequently, in the induction of the Unfolded Protein response (UPR) in mammalian cells (14, 16). Therefore, 2DG interferes with several cellular functions.

In this study, we used mass spectrometry as an unbiased approach to describe the cellular effects of 2DG on the total cellular proteome. This revealed that many glycolytic enzymes are upregulated, likely as a consequence of an impaired glycolysis.

A second and unexpected observation was to identify, within the list of 2DG-upregulated proteins, the Dog1 and/or Dog2 phosphatase, previously involved in 2DG resistance (33, 40, 41). Our subsequent results on the relative abundance of Dog1 and Dog2 suggest that the protein identified by mass spectrometry, which could not be discriminated at this stage because of the high identity between these paralogues, is likely to be Dog2. Dog2 upregulation upon 2DG treatment was intriguing because it wasn't clear how a synthetic molecule such as 2DG could trigger the onset of a resistance mechanism. It should be noted that the cellular functions of Dog1/Dog2, beyond 2DG dephosphorylation, are unknown. They can dephosphorylate a range of phosphorylated sugars *in vitro* (40), in agreement with the fact that other members of the HAD family of phosphatases can accommodate various substrates (77). Therefore, it seemed plausible that Dog1/2 induction was a response to one or more of the cellular consequences of 2DG treatment, and not to 2DG itself. Our study reveals that actually, the expression of Dog1 and Dog2 is controlled by multiple signaling

pathways, each of which are turned on as a response to 2DG (see Working model, **Figure 9**). This study was also taken as an opportunity to probe the signaling pathways that are activated upon 2DG exposure and precise the causes of these activations.

First, we showed that Dog1 and Dog2 are induced by ER stress. We confirmed that 2DG triggers ER stress and the onset of the UPR pathway. This was not unexpected given the proposed mode of action of this drug and the available data in the literature on mammalian cells (14, 16), but this had not been formally proven in yeast with current tools. The induction of an UPR reporter and the hypersensitivity of UPR mutant strains such as *hac1*Δ or *ire1*Δ are in agreement with this conclusion. Finally, the hypersensitivity phenotype of UPR mutants to 2DG could be alleviated by restoring N-glycosylation through the addition of mannose in the culture medium, suggesting that 2DG toxicity in UPR mutants is directly due to defects in protein N-glycosylation. These results are in line with high-throughput studies proposing that both *DOG1* and *DOG2* are UPR-regulated genes (88).

Second, we showed that 2DG also activates the MAP kinase-based cell wall integrity (CWI) pathway. Several studies reported connections between ER stress signaling and the CWI pathway (56-60), and 2DG-elicited N-glycosylation and ER stress may have repercussions on the CWI pathway. For instance, it was previously observed that CWI pathway mutants are sensitive to tunicamycin because they lack an ER surveillance-pathway which normally prevents the inheritance of stressed ER (58). Many CWI mutants were indeed sensitive to low concentrations (0.05%) of 2DG but unlike UPR mutants, their growth was not restored by the addition of exogenous mannose, suggesting that N-glycosylation defect is not the sole reason why CWI mutants are sensitive to 2DG. 2DG was also shown to interfere with the synthesis of structural polysaccharides that make up the yeast cell wall (mannans and glucans), again because 2DG acts as an antagonist of mannose but also of glucose incorporation into these polymers (42, 89-91). Accordingly, 2DG exposure leads to yeast cell lysis at sites of growth, which is where glucan synthesis occurs (43) and where the major glucan synthase, Fks1, is localized (92). Thus, we propose that 2DG-induced weakening of the cell wall could be responsible for the triggering of the cell wall integrity pathway (**Figure 9**). This could explain why the main sensors responsible for

sensing cell wall damage, Wsc1 and Mid2 (reviewed in 55), are required for growth on 2DG. In addition, we also report that Dog1 and Dog2 are less expressed in CWI mutants, which could further sensitize these strains to 2DG. Although the effect of 2DG on cell wall synthesis applies to fungi but not to animal cells that do not harbor a cell wall, it denotes the interference of 2DG with UDP-glucose metabolism that is likely to be conserved in animals (93). 2DG may affect metabolic pathways involving these precursors in metazoans, such as glycogen synthesis (94, 95). Additionally, 2DG was shown to be metabolized into GDP-glucose, which incorporates into dolichol-phosphate precursors and further interferes with protein glycosylation (90, 96), but also into phosphoinositol-based lipids (97), the cellular consequences of which are unknown.

Our data also reveal that the increased 2DG-6-phosphate phosphatase activity of the *reg1* mutants, that has been described very early on (28, 38, 39), is partly due to the glucose-mediated repression of Dog2, the latter being consequently overexpressed in the *reg1Δ* mutant. This may also contribute to the 2DG resistance of *hxk2* and *mig1* mutants, which also act in the glucose-repression pathways and were identified in previous screens (29, 35). Indeed, we show that the 2DG resistance displayed by the *reg1Δ* and *hxk2Δ* strains was partially due to an increased expression of Dog2. In the *hxk2Δ* mutant, the lack of hexokinase 2 is compensated by the expression of other glucose-phosphorylating enzymes (such as Hxk1 and glucokinase, Glk1) (98) that may be less prone to phosphorylate 2DG (36), and thus could lead to a lower accumulation of 2DG6P in the cell and further increase 2DG resistance. Hxk2 also has additional, non-metabolic roles beyond sugar phosphorylation, whose loss may additionally contribute to this phenotype (reviewed in Ref. 99). Concerning the *reg1*Δ strain, the additional mechanisms of resistance also remain to be investigated. A cross-talk between the Snf1/Reg1 couple and the UPR pathway has been described (63, 64), however these studies revealed that the *reg1Δ* mutant is actually hypersensitive to UPR inducers such as tunicamycin (**Figure 5B**) (63, 64), making its resistance towards 2DG (which is also an UPR inducer) even more striking. What appeared from previous work is that the resistance of the *reg1Δ* mutant is dependent on Snf1 hyperactivity, since the additional deletion of *SNF1* restores 2DG sensitivity to the *reg1Δ* strain (31). Thus, additional yet Snf1-

dependent mechanisms cooperate with the increased expression of *DOG2* to allow *reg1Δ* cells to resist to 2DG.

After 2DG import and phosphorylation, the amount of 2DG6P in cells can exceed that of G6P by up to 80-fold (100). Overexpression of Dog2 was previously shown to revert the repressive effect of 2DG (33), suggesting that it can clear the 2DG6P pool up to a point where 2DG6P is no longer detected by the yet unknown cellular glucose-sensing mechanism. Thus, Dog2 overexpression appears as a good strategy for 2DG resistance, and indeed, it was overexpressed in the majority of the spontaneous resistant mutants we isolated. This included mutants in the *REG1* and *HXK2* genes, but additionally, we identified two mutants carrying a point mutation in the gene encoding the transcriptional repressor Cyc8, leading to a truncated protein at codon 320, within its 8th predicted tetratricopeptide (TPR) repeat. The TPR repeats are involved in the interaction of Cyc8 with its co-repressor Tup1, and to specify its recruitment to specific promoters, possibly through the recruitment of pathway-specific DNA-binding proteins (101). The identified truncation leads to the de-repression of invertase and Dog2, but does not impact on growth as strongly as the full deletion of the gene. Interestingly, recent data showed that point mutations in TPR units 9 and 10 affect Cyc8 function in a similar manner as the mutation we isolated (i.e. impact on glucose repression but not global growth), suggesting that alterations at this region affect a subset of Cyc8 functions (102). This is in line with a study showing the differential requirement of TPR repeats for the various functions of Cyc8, and in particular the involvement of the TPR repeats 8-10 in glucose repression (103). Altogether, these data describe *DOG2* overexpression as a successful strategy to overcome 2DG toxicity.

Similarly, the selection of HeLa-derived 2-DG-resistant cell lines showed an increase in 2DG6P phosphatase activity, but the responsible enzyme was not identified (20). Based on sequence similarity, we identified HDHD1 as an enzyme displaying *in vitro* 2DG6P phosphatase activity and whose overexpression in both yeast and HeLa cells allows resistance to 2DG. Actually, we found that HDHD1 has a very low affinity toward 2DG (in the 10^{-2} M range, unpublished data) as compared to other substrates such as 5'-pseudouridine monophosphate or even 3'-AMP (79). Despite this very low

affinity for 2DG, HDHD1 overexpression in HeLa cells conferred resistance to 2DG. Whether HDHD1 is responsible for the 2DG resistance previously reported in human cells (20) remains to be investigated.

Altogether, our work shows that 2DG-induced activation of multiple signaling pathways can rewire the expression of endogenous proteins which can target 2DG6P to promote 2DG tolerance, and whose deregulated expression can lead to 2DG resistance. This mechanism likely superimposes on other resistance mechanisms that should be scrutinized in the future.

Acknowledgments.

We would like to thank Nicolas Joly for discussion about the HDHD1 *in vitro* assay, Gaelle Lelandais for help with Yeastract analysis, Pascual Sanz and Jose Antonio Prieto for the gift of the GST-Dog2 construct, Emile Van Schaftingen for the gift of the His-tagged HDHD1 construct, Peter Walter for the gift of the *pUPRE1*:lacZ reporter, David Levin for the gift of the pCYC(2xRlm1):lacZ reporter, Colin Stirling for the gift of the anti-invertase antibody and Martin Schmidt for advice regarding gDNA extraction for sequencing. We also thank Thibaut Léger and the Proteomics facility of the Institut Jacques Monod (supported by the Region Ile-de-France (SESAME), the Paris-Diderot University (ARS), and CNRS) for assistance. We thank Anna Babour, Myriam Ruault and members of the Léon lab for insightful comments and critical reading. This work was supported by fellowships from the Fondation pour la Recherche Médicale (SPF20150934065 to QD) and the Ligue contre le cancer (TAZK20115 to CL), and by grants from the Agence Nationale pour la Recherche (P-Nut, ANR-16-CE13-0002 to SL) and the Fondation ARC pour la recherche sur le cancer (PJA20181208080 to SL).

Material and Methods

Yeast strain construction and growth conditions

All yeast strains used in this study derive from the *Saccharomyces cerevisiae* BY4741 or BY4742 background and are listed in **Supplemental Table S3**. Apart from the mutant strains obtained from the yeast deletion collection (Euroscarf) and the fluorescent GFP tagged strains originating from the yeast GFP clone collection (104), all yeast strains were constructed by transformation with the standard lithium acetate-polyethylene glycol protocol using homologous recombination and verified by PCR on genomic DNA prepared with a lithium acetate (200mM) / SDS (0.1%) method (105).

Yeast cells were grown in YPD medium (Yeast extract-Peptone-Dextrose 2%) or in synthetic complete medium (SC, containing 1.7g/L yeast nitrogen base (MP Biomedicals), 5g/L ammonium sulfate (Sigma-Aldrich), the appropriate drop-out amino acid preparations (MP Biomedicals) and 2% (w/vol) glucose unless otherwise indicated). Alternatively, SC medium could contain 0.5% lactate as a carbon source (from a 5% stock adjusted to pH=5; Sigma Aldrich). Pre-cultures of 4mL were incubated at 30°C for 8 hours and diluted in fresh medium on the evening to 20mL cultures grown overnight with inoculation optical densities (OD_{600}) of 0.0003 for YPD and 0.001 for SC medium, giving a culture at mid-log phase the next morning.

For glucose depletion experiments, cultures were centrifuged and resuspended in an equal volume of SC/lactate medium and incubated at 30°C during the indicated times. For 2-deoxyglucose, NaCl and tunicamycin treatments, the compounds were added to mid-log phase yeast cultures grown overnight to respective final concentrations of 0.2% (w/v), 400mM and 1µg/mL and incubated for the indicated times. 2-deoxyglucose and tunicamycin were purchased from Sigma-Aldrich. The mannose-supplemented medium (Fig. 2B) consisted of an SC medium that contained all the element indicated above plus 2% (w/vol) mannose.

Plasmid construction

All the plasmids presented in this study are listed in **Supplemental Table S4** and were directly constructed in yeast using plasmid homologous recombination (106). DNA inserts were amplified by PCR using 70-mer primers containing 50nt homology overhangs and Thermo Fisher Phusion High-fidelity DNA Polymerase and receiver plasmids were digested with restriction enzymes targeting the insertion region. Competent yeast cells rinsed with lithium acetate were incubated for 30 minutes at 30°C with 20µL of the PCR product and 1µL of the plasmid digestion product, followed by a heat shock at 42°C for 20 minutes and a recovery phase in rich medium (YPD) for 90 minutes at 30°C and plated on synthetic medium without uracil. The pDOG1/2-LacZ vectors were generated using the pJEN1-LacZ

vector obtained from Bernard Guiard (107) and cloning the pDOG1 or pDOG2 promoters (1kb) at *Bgl*II and *Eco*RI sites.

The *DOG1*, *DOG2*, *HDHD1* (all four isoforms), *HDHD4*, *PSPH* and *yniC* overexpression vectors were obtained by digesting a pRS426 vector (2µ, *URA3*) containing the p*GPD* promoter with *Eco*RI and *Bam*HI enzymes. In parallel, inserts were PCR-amplified using the following DNA templates: *DOG1* and *DOG2* from yeast genomic DNA preparations (primers: oSL1166/1167 and oSL1141/1142), the *yniC* ORF from *Escherichia coli* DH5α cells (oSL1172/1173) and the human gene ORFs (Uniprot identifiers: HDHD1=Q08623-1/2/3/4, HDHD4=Q8TBE9 and PSPH=P78330) from DNA sequences generated by gene synthesis after codon optimization for yeast expression (Eurofins Genomics) (*HDHD1*: oSL1170/1171 for all isoforms except isoform 3: oSL1170/1216; *HDHD4*: oSL1214/1215; *PSPH*: oSL1212/1213). These PCR products were designed to include a 50-bp overlap with the digested plasmid so as to clone them by homologous recombination in yeast after co-transformation. The p*GPD-HDHD1*-DDAA vector was obtained by PCR amplification (oSL1155/1171) of the *HDHD1* DNA sequence obtained by gene synthesis using a specific 5' primer carrying two D>A mutations and insertion of this insert into the pRS426 vector digested with EcoRI and BamHI as described above. This construct was verified by sequencing. The DDAA mutant was PCR amplified (oSL1297/oSL1298) and subcloned at NdeI/BamHI sites into pET15b-6His-HDHD1, a kind gift of Dr. E. Van Schaftingen, to substitute for endogenous HDHD1.

Plasmids expressing the wild-type *CYC8* gene and the mutant allele present in mutant #9 were obtained by PCR amplification on the corresponding genomic DNAs with primers (oSL1369/1370) containing a 50-bp overlap with a pRS415 vector (CEN, *LEU2*) digested with XbaI and BamHI, and co-transformation for cloning by homologous recombination in yeast as described above.

The plasmids generated in yeast were rescued by extraction (lithium acetate/SDS method (105)) and electroporation in bacteria, then amplified and sequenced before being re-transformed in the appropriate strains.

Mass spectrometry and proteomics analyses

Samples used for the proteome-wide analysis of 2-deoxyglucose treatments were prepared from six liquid cultures (WT strain, BY4741) growing overnight at 30°C in 100mL of rich medium with 2% glucose to mid-log phase. On the next morning, 2-deoxyglucose was added to three of the cultures to a final concentration of 0.2% in order to obtain triplicates treated with 2-DG and triplicates without drug treatment (negative control). After 2.5 hours of incubation at 30°C, the six cultures were centrifuged at 4000*g* for 5 minutes at 4°C, resuspended in 500*µ*L of 10% trichloroacetic acid (TCA, Sigma-Aldrich) and lysed by shaking after addition of glass beads (0.4-0.6mm, Sartorius) for 10 minutes at 4°C. Cell lysates were retrieved by piercing under the 1.5mL tubes and brief centrifugation. Precipitated

proteins were centrifuged at 16000*g* for 10 minutes at 4°C, supernatants were discarded and pellets were rinsed 4 times in 1mL of 100% cold acetone.

Proteins were then digested overnight at 37°C in 20 µL of 25 mM NH_4HCO_3 containing sequencing-grade trypsin (12.5 µg/mL; Promega). The resulting peptides were sequentially extracted with 70% acetonitrile, 0.1% formic acid. Digested samples were acidified with 0.1% formic acid. All digests were analyzed by an Orbitrap Fusion equipped with an EASY-Spray nanoelectrospray ion source and coupled to an Easy nano-LC Proxeon 1000 system (all from Thermo Fisher Scientific, San Jose, CA). Chromatographic separation of peptides was performed with the following parameters: Acclaim PepMap100 C18 pre-column (2 cm, 75 µm i.d., 3 µm, 100 Å), Pepmap-RSLC Proxeon C18 column (50 cm, 75 µm i.d., 2 µm, 100 Å), 300 nl/min flow, using a gradient rising from 95 % solvent A (water, 0.1 % formic acid) to 40 % B (80 % acetonitrile, 0.1% formic acid) in 120 minutes, followed by a column regeneration of 20 min, for a total run of 140 min. Peptides were analyzed in the orbitrap in full-ion scan mode at a resolution of 120,000 (at *m/z* 200) and with a mass range of *m/z* 350-1550, and an AGC target of $2x10^5$. Fragments were obtained by higher-energy C-trap dissociation (HCD) activation with a collisional energy of 30 %, and a quadrupole isolation window of 1.6 Da. MS/MS data were acquired in the linear ion trap in a data-dependent mode, in top-speed mode with a total cycle of 3 seconds, with a dynamic exclusion of 50 seconds and an exclusion duration of 60 seconds. The maximum ion accumulation times were set to 250 ms for MS acquisition and 30 ms for MS/MS acquisition in parallelization mode.

Raw mass spectrometry data from the Thermo Fisher Orbitrap Fusion were analyzed using the MaxQuant software (108) version 1.5.0.7, which includes the Andromeda peptide search engine (109). Theoretical peptides were created using the *Saccharomyces cerevisiae* S288C proteome database obtained from Uniprot. Identified spectra were matched to peptides with a main search peptide tolerance of 6ppm. After filtering of contaminants and reverse identifications, the total amount of yeast proteins identified among the six samples was equal to 3425. Protein quantifications were performed using MaxLFQ (110) on proteins identified with a minimum amount of two peptides with a False Discovery Rate threshold of 0.05. LFQ values were then analyzed using Perseus (version 1.5.0.15). For the statistical analysis of yeast proteomes treated with 2-dexogylucose compared to negative control samples, each group of triplicates was gathered into a statistical group in order to perform a Student's t-test. Results are presented in the form of Volcano-plots (111) and significant up-regulated and down-regulated candidates were determined by setting an FDR of 0.01 and an S_0 of 2.

GO-term analyses of proteomics data

The 79 significantly up-regulated candidates obtained in the proteomics analysis were used as input for the FunSpec web interface (http://funspec.med.utoronto.ca/) with default settings and a p-value

cutoff of 0.01 in order to determine the Gene Ontology biological processes that are enriched in this list of 79 genes compared to the total *Saccharomyces cerevisiae* genome annotation (number of total categories=2062). The complete list of enriched GO biological processes with a p-value<0.01, as well as the genes included in each category, are displayed in Supplemental Figure S1A.

Protein extracts and immunoblotting

Yeast cultures used for protein extracts were all grown in synthetic complete medium. For each protein sample, 1.4mL of culture was incubated with 100µL of 100% TCA for 10 minutes on ice to precipitate proteins, centrifuged at 16000*g* at 4°C for 10 minutes and broken for 10 minutes with glass beads, as described for LC-MS/MS sample preparation. Lysates were transferred to another 1.5mL tube and centrifuged 5 minutes at 16000*g* at 4°C, supernatants were discarded and protein pellets were resuspended in 50µL*(OD_{600} of the culture) of sample buffer (50 mM Tris-HCl pH6.8, 100 mM DTT, 2% SDS, 0.1% bromophenol blue, 10% glycerol, complemented with 50mM Tris-Base pH8.8). Protein samples were heated at 95°C for 5 minutes and 10µL were loaded on SDS-PAGE gels (4-20%Mini-PROTEAN TGX Stain-Free, BioRad). After electrophoresis, gels were blotted on nitrocellulose membranes for 60 minutes with a liquid transfer system (BioRad), membranes were blocked in 2% milk for 20 minutes and incubated for at least two hours with the corresponding primary antibodies. Primary and secondary antibodies used in this study as well as their dilutions are listed in **Supplemental Table S5**. Membranes were washed three times for 10 minutes in Tris-Borate-SDS-Tween20 0.5% buffer and incubated for at least an hour with the corresponding secondary antibody (coupled with Horse Radish Peroxidase). Luminescence signals were acquired with the LAS-4000 imaging system (Fujifilm). Rsp5 was used as a loading control; alternatively, total proteins were visualized in gels using a trihalo compound incorporated in SDS–PAGE gels (stain-free TGX gels, 4–20%; Bio-Rad) after 1 min UV-induced photoactivation and imaging using a Gel Doc EZ Imager (Bio-Rad).

Beta-galactosidase assays

β-Galactosidase assays were performed using 1mL of mid-log phase yeast cultures carrying the p_{DOG1}-*LacZ* or p_{DOG2}-*LacZ* plasmids, grown overnight in SC medium without uracil with glucose 2% and switched to the specified conditions. The OD (600 nm) of the culture was measured, and samples were taken and centrifuged at 16000*g* at 4°C for 10 minutes, cell pellets were snap frozen in liquid nitrogen and resuspended in 800µL of Buffer Z (pH=7, 50mM NaH_2PO_4, 45mM Na_2HPO_4, 10mM $MgSO_4$, 10mM KCl and 38mM β-mercaptoethanol). After addition of 160µL of 4mg/mL ONPG (ortho-nitrophenyl-β-D-galactopyranoside, Sigma-Aldrich), samples were incubated at 37°C. Enzymatic reactions were stopped in the linear phase (60min incubation for p_{DOG2}-*LacZ* and 120min incubation for the p_{DOG1}-*LacZ* plasmid, as per initial tests) by addition of 400µL of Na_2CO_3, and cell debris were discarded by

centrifugation at 16000*g*. The absorbance of clarified samples was measured with a spectrophotometer set at 420nm. β-Galactosidase activities (arbitrary units, AU) were calculated using the formula 1000*[A_{420}/(A_{600}* t)], where A_{420} refers to the enzyme activity and A600 is the turbidity of the culture, and t the incubation time. Each enzymatic assay was repeated independently at least three times.

Drop tests

Yeast cells grown in liquid rich or synthetic complete medium for at least 6 hours at 30°C were adjusted to an optical density (600nm) of 0.5. Five serial 10-fold dilutions were prepared in 96-well plates and, using a pin replicator, drops were spotted on plates containing rich or SC medium containing 2% (w/v) agar and when indicated, 2DG (0.05%, or 0.2%, w/vol), sodium selenite (200µM) or tunicamycin (1µg/mL). Plates containing mannose (Fig 2H and 3G) were prepared as regular SC plates into which 2% mannose (w/vol) was added. Plates were incubated at 30°C for 3 to 4 days before scanning. For the adhesion test (Figure 6C), the plates were scanned and the colonies were then washed with tap water under a constant flow of water for 1 min as previously described (74). Excess water was removed before the plates were scanned again.

2-NBDG treatment and Fluorescence microscopy

For 2-NBDG treatments, yeast cells were grown overnight in SC medium containing 2% glucose to the exponential phase, then switched to SC medium with 0.5% lactate and incubated at 30°C for 30 minutes. This allowed the clearance of glucose from the medium, without which 2NBDG import was too weak to be observed since Glucose and 2NBDG compete for transport (112). 2NBDG (2-(*N*-(7-Nitrobenz-2-oxa-1,3-diazol-4-yl)Amino)-2-Deoxyglucose; Cayman Chemical) was then added at a concentration of 300µM for the indicated times.

Yeast were then rinsed twice in 1mL of cold water before being mounted on a glass slide and imaged at 25°C with a BX-61 fluorescence microscope (Olympus) equipped with a PlanApo 1.40NA 100X objective (Olympus), a QiClick monochrome camera (QImaging) and acquired using the MetaVue software (Molecular Devices). The 2-NBDG signal was visualized using a GFP filter set (41020 from Chroma Technology, Bellows Falls, VT; excitation HQ480/20X, dichroic Q505LP, emission HQ535/50m). Loa1-mCherry was visualized using an HcRedI filter set (41043 from Chroma Technology, Bellows Falls, VT; excitation HQ575/50X, dichroic Q610lp, emission HQ640/50m). Images were opened with ImageJ and processed for cropping and equivalent contrast adjustment.

Isolation of spontaneous mutants and characterization.

WT cells transformed with a p*DOG2*-LacZ plasmid (pSL410) were grown overnight in SC-Ura medium and ca. 2x10(6) cells were spread on SC-Ura plates containing 0.2% 2DG and grown for 6 days at 30°C.

The clones obtained (24 clones) were restreaked on SC-Ura to isolate single clones. Resistance to 2DG was confirmed by drop tests (see **Figure 5B**). Beta-galactosidase enzyme assays and total protein extracts were performed on cultures grown to the exponential phase. For beta-galactosidase assays, the results of three independent experiments are shown along and were statistically tested using an unpaired t-test with equal variance.

Diploids were obtained by crossing each resistant mutant with a WT or *hxk2Δ* strain of the opposite mating type (BY4742, Matα) and selecting single diploid clones on selective medium (SC-Met-Lys). Sequencing of the *REG1* and *HXK2* loci were done after PCR amplification on genomic DNA isolated from the corresponding clones. For whole genome sequencing, genomic DNA of the WT, clone 9 and clone 10 was purified using the Qiagen genomic DNA kit (Genomic-tip 20/G) using 30 OD equivalents of material following the manufacturer's instructions after zymolyase treatment (Seikagaku). A PCR-free library was generated from 10 µg of gDNA and sequenced at the Beijing Genomics Institute (Hong Kong) on Illumina HiSeq 4000. The mutations in each clone were identified through comparative analysis of the variants detected by mapping their reads to the reference genome (BY4741) (113, 114) and those detected by mapping the WT reads to the reference. The differential variants were filtered by quality (vcf QUAL>1000) and manually inspected through IGV for validation (115).

Cell culture and transfection.

HeLa cells were maintained at 37°C and 5% CO_2 in a humidified incubator and grown in Dulbecco's modified Eagle's medium (DMEM), supplemented with 10% fetal calf serum (FCS). Cells were regularly split using Trypsin-EDTA to maintain exponential growth. HeLa cells were transfected with plasmid pCMV-Sport6-HDHD1 and pCS2 (empty control) using Lipofectamine 2000 according to the manufacturer's instructions. All culture media reagents were from Thermo Fisher Scientific. 2DG (Sigma) was used at a final concentration of 5 mM and tunicamycin (from *Streptomyces sp;* Sigma) was used at a final concentration of 5 µg/mL. For 2DG resistance assays, cells were grown in 10 cm2 flask and split in a 24-well plate in the absence or presence of 5 mM 2DG. Cells were counted each day with a hemocytometer after trypsinization and labeling with Trypan Blue. Total extracts were prepared by incubating cells (10 cm2) on ice for 20 min with 400 µL TSE Triton buffer (50 mM Tris- HCl pH 8.0, NaCl 150 mM, 0.5 mM EDTA, 1% Triton X-100) containing protease inhibitors (cOmplete protease inhibitor cocktail, EDTA-Free, Roche Diagnostics). Cells were then lysed mechanically with scrapers, and the lysate was centrifuged at 13,000 g, 4°C for 30 min. Proteins were assayed in the supernatant using the Bio-Rad Protein Assay reagent (Bio-Rad) and 40 µg proteins were loaded on SDS-PAGE gels.

Recombinant His-tagged HDHD1 and HDHD1-DDAA protein purifications

E. coli BL21 bacteria were transformed with plasmids allowing the expression of His-tagged HDHD1 or HDHD1-DDAA . A 100mL-preculture was grown overnight in LB+Ampicillin (100 µg/mL), diluted 50-fold into 1L culture. The OD reached 0.7-0.9. IPTG (1 mM) was then added to induce the recombinant protein and cells were further grown at 25°C for 3 hours. Cells were harvested, the pellet was frozen in liquid N_2 and thawed on ice. The pellet was resuspended in 20 mL of lysis buffer (HEPES 25mM pH 6.7, 300mM NaCl, imidazole 15 mM, beta-mercaptoethanol 2mM, glycerol 10% v/v and protease inhibitor cocktail [cOmplete protease inhibitor cocktail, EDTA-Free, Roche Diagnostics]). Cells were then sonicated and Triton X-100 was added to a final concentration of 1%. The lysate was centrifuged at 12,000rpm in a SW-32 rotor (Beckman Coulter) for 15min at 4°C, and then the supernatant was further centrifuged at 35 000 rpm for 1h at 4°C. The supernatant was incubated with 800 µL of Ni-NTA beads slurry (Qiagen) and rotated overnight at 4°C. The beads were collected by centrifugation (1000*g*, 2min, 4°C), resuspended in lysis buffer, and washed with 50 mL of lysis buffer at 4°C, and then washed again with 50 mL thrombin cleavage buffer (Hepes 50 mM, $CaCl_2$ 5 mM, NaCl 100mM, glycerol 10%) at 4°C. The His-tag was removed by cleavage with 16 U of thrombin (Ref 27-0846-01, Sigma) added directly onto the beads for 2h at 25°C. The eluate was then collected and incubated with 500 µL benzamidin-sepharose 6B (GE Healthcare) at room temperature for 30 min to remove thrombin. The supernatant was collected and protein content was assayed by SDS-PAGE and colloidal blue staining (Brilliant Blue G-colloidal, Sigma), and protein concentration was assayed by the Bradford method (Bio-Rad protein assay, Bio-Rad).

Enzyme assays

2-DG-6-Phosphate phosphatase assays were performed in 250 µL of reaction containing 1.5mM 2-DG-6-Phosphate (#17149, Cayman Chemicals, Ann Arbor, Michigan, USA) in 50 mM HEPES pH 6.7, 10 mM $MgCl_2$ and 10% glycerol and 30 µg recombinant HDHD1 or HDHD1-DDAA. Samples were incubated at 37°C for various times (0, 5, 10, 15min) and the reaction was stopped by adding 150µL EDTA (0.5M). Then, the 2-deoxyglucose generated was assayed by adding 500µL of glucose assay reagent (GAGO20, Sigma) and further incubating at 37°C for 30min. The reaction was stopped by adding 500µL H_2SO_4 (12N) and the absorbance of the reaction was measured at 540 nm. A slope (A540 over time) was calculated to access to the enzyme activity and allowed to see that the reaction was in the linear range. The measurements were repeated 3 times.

Statistical analysis

Mean values calculated using a minimum of three independent measurements from three biological replicates and are plotted with error bars representing standard error of the mean (SEM). Statistical

1 significance was determined using a t-test for paired variables, as follows: *: $P \leq 0.05$; **: $P \leq 0.01$;

2 ***: $P \leq 0.001$; ns: $P > 0.05$.

References

1. Kroemer G, Pouyssegur J. Tumor cell metabolism: cancer's Achilles' heel. Cancer cell. 2008;13(6):472-82.
2. Yun J, Rago C, Cheong I, Pagliarini R, Angenendt P, Rajagopalan H, et al. Glucose deprivation contributes to the development of KRAS pathway mutations in tumor cells. Science. 2009;325(5947):1555-9.
3. Pelicano H, Martin DS, Xu RH, Huang P. Glycolysis inhibition for anticancer treatment. Oncogene. 2006;25(34):4633-46.
4. Galluzzi L, Kepp O, Vander Heiden MG, Kroemer G. Metabolic targets for cancer therapy. Nature reviews Drug discovery. 2013;12(11):829-46.
5. Karczmar GS, Arbeit JM, Toy BJ, Speder A, Weiner MW. Selective depletion of tumor ATP by 2-deoxyglucose and insulin, detected by 31P magnetic resonance spectroscopy. Cancer Res. 1992;52(1):71-6.
6. Chen W, Gueron M. The inhibition of bovine heart hexokinase by 2-deoxy-D-glucose-6-phosphate: characterization by 31P NMR and metabolic implications. Biochimie. 1992;74(9-10):867-73.
7. Sols A, Crane RK. Substrate specificity of brain hexokinase. J Biol Chem. 1954;210(2):581-95.
8. Wick AN, Drury DR, Nakada HI, Wolfe JB. Localization of the primary metabolic block produced by 2-deoxyglucose. J Biol Chem. 1957;224(2):963-9.
9. Zhang D, Li J, Wang F, Hu J, Wang S, Sun Y. 2-Deoxy-D-glucose targeting of glucose metabolism in cancer cells as a potential therapy. Cancer Lett. 2014;355(2):176-83.
10. Stein M, Lin H, Jeyamohan C, Dvorzhinski D, Gounder M, Bray K, et al. Targeting tumor metabolism with 2-deoxyglucose in patients with castrate-resistant prostate cancer and advanced malignancies. Prostate. 2010;70(13):1388-94.
11. Dwarakanath BS, Singh D, Banerji AK, Sarin R, Venkataramana NK, Jalali R, et al. Clinical studies for improving radiotherapy with 2-deoxy-D-glucose: present status and future prospects. J Cancer Res Ther. 2009;5 Suppl 1:S21-6.
12. Raez LE, Papadopoulos K, Ricart AD, Chiorean EG, Dipaola RS, Stein MN, et al. A phase I dose-escalation trial of 2-deoxy-D-glucose alone or combined with docetaxel in patients with advanced solid tumors. Cancer Chemother Pharmacol. 2013;71(2):523-30.
13. Szablewski L. Expression of glucose transporters in cancers. Biochim Biophys Acta. 2013;1835(2):164-9.
14. Kurtoglu M, Gao N, Shang J, Maher JC, Lehrman MA, Wangpaichitr M, et al. Under normoxia, 2-deoxy-D-glucose elicits cell death in select tumor types not by inhibition of glycolysis but by interfering with N-linked glycosylation. Molecular cancer therapeutics. 2007;6(11):3049-58.
15. Andresen L, Skovbakke SL, Persson G, Hagemann-Jensen M, Hansen KA, Jensen H, et al. 2-deoxy D-glucose prevents cell surface expression of NKG2D ligands through inhibition of N-linked glycosylation. J Immunol. 2012;188(4):1847-55.
16. Lin HY, Masso-Welch P, Di YP, Cai JW, Shen JW, Subjeck JR. The 170-kDa glucose-regulated stress protein is an endoplasmic reticulum protein that binds immunoglobulin. Mol Biol Cell. 1993;4(11):1109-19.
17. Xi H, Kurtoglu M, Liu H, Wangpaichitr M, You M, Liu X, et al. 2-Deoxy-D-glucose activates autophagy via endoplasmic reticulum stress rather than ATP depletion. Cancer Chemother Pharmacol. 2011;67(4):899-910.
18. Pietzke M, Zasada C, Mudrich S, Kempa S. Decoding the dynamics of cellular metabolism and the action of 3-bromopyruvate and 2-deoxyglucose using pulsed stable isotope-resolved metabolomics. Cancer Metab. 2014;2:9.
19. Kavaliauskiene S, Skotland T, Sylvanne T, Simolin H, Klokk TI, Torgersen ML, et al. Novel actions of 2-deoxy-D-glucose: protection against Shiga toxins and changes in cellular lipids. Biochem J. 2015;470(1):23-37.

20. Barban S. Studies on the mechanism of resistance to 2-deoxy-D-glucose in mammalian cell cultures. J Biol Chem. 1962;237:291-5.
21. Diaz-Ruiz R, Rigoulet M, Devin A. The Warburg and Crabtree effects: On the origin of cancer cell energy metabolism and of yeast glucose repression. Biochim Biophys Acta. 2011;1807(6):568-76.
22. Celenza JL, Carlson M. A yeast gene that is essential for release from glucose repression encodes a protein kinase. Science. 1986;233(4769):1175-80.
23. Nehlin JO, Ronne H. Yeast MIG1 repressor is related to the mammalian early growth response and Wilms' tumour finger proteins. EMBO J. 1990;9(9):2891-8.
24. Lutfiyya LL, Johnston M. Two zinc-finger-containing repressors are responsible for glucose repression of SUC2 expression. Mol Cell Biol. 1996;16(9):4790-7.
25. Conrad M, Schothorst J, Kankipati HN, Van Zeebroeck G, Rubio-Texeira M, Thevelein JM. Nutrient sensing and signaling in the yeast Saccharomyces cerevisiae. FEMS Microbiol Rev. 2014;38(2):254-99.
26. Zimmermann FK, Scheel I. Mutants of Saccharomyces cerevisiae resistant to carbon catabolite repression. Mol Gen Genet. 1977;154(1):75-82.
27. Bailey RB, Woodword A. Isolation and characterization of a pleiotropic glucose repression resistant mutant of Saccharomyces cerevisiae. Mol Gen Genet. 1984;193(3):507-12.
28. Heredia MF, Heredia CF. Saccharomyces cerevisiae acquires resistance to 2-deoxyglucose at a very high frequency. J Bacteriol. 1988;170(6):2870-2.
29. Neigeborn L, Carlson M. Mutations causing constitutive invertase synthesis in yeast: genetic interactions with snf mutations. Genetics. 1987;115(2):247-53.
30. Ralser M, Wamelink MM, Struys EA, Joppich C, Krobitsch S, Jakobs C, et al. A catabolic block does not sufficiently explain how 2-deoxy-D-glucose inhibits cell growth. Proc Natl Acad Sci U S A. 2008;105(46):17807-11.
31. McCartney RR, Chandrashekarappa DG, Zhang BB, Schmidt MC. Genetic analysis of resistance and sensitivity to 2-deoxyglucose in Saccharomyces cerevisiae. Genetics. 2014;198(2):635-46.
32. Witt I, Kronau R, Holzer H. Repression von Alkoholdehydrogenase, Malatdehydrogenase, Isocitratlyase und Malatsynthase in Hefe durch Glucose. Biochim Biophys Acta. 1966;118(3):522-37.
33. Randez-Gil F, Prieto JA, Sanz P. The expression of a specific 2-deoxyglucose-6P phosphatase prevents catabolite repression mediated by 2-deoxyglucose in yeast. Current genetics. 1995;28(2):101-7.
34. Hedbacker K, Carlson M. Regulation of the nucleocytoplasmic distribution of Snf1-Gal83 protein kinase. Eukaryot Cell. 2006;5(12):1950-6.
35. Schuller HJ, Entian KD. Extragenic suppressors of yeast glucose derepression mutants leading to constitutive synthesis of several glucose-repressible enzymes. J Bacteriol. 1991;173(6):2045-52.
36. Lobo Z, Maitra PK. Physiological role of glucose-phosphorylating enzymes in Saccharomyces cerevisiae. Arch Biochem Biophys. 1977;182(2):639-45.
37. Maitra PK. A glucokinase from Saccharomyces cerevisiae. J Biol Chem. 1970;245(9):2423-31.
38. Heredia CF, Sols A. Metabolic Studies with 2-Deoxyhexoses. II. Resistance to 2- Deoxyglucose in a Yeast Mutant. Biochim Biophys Acta. 1964;86:224-8.
39. Martin M, Heredia CF. Characterization of a phosphatase specific for 2-deoxyglucose-6-phosphate in a yeast mutant. FEBS Lett. 1977;83(2):245-8.
40. Randez-Gil F, Blasco A, Prieto JA, Sanz P. DOGR1 and DOGR2: two genes from Saccharomyces cerevisiae that confer 2-deoxyglucose resistance when overexpressed. Yeast. 1995;11(13):1233-40.
41. Sanz P, Randez-Gil F, Prieto JA. Molecular characterization of a gene that confers 2-deoxyglucose resistance in yeast. Yeast. 1994;10(9):1195-202.
42. Heredia CF, de la Fuente G, Sols A. Metabolic Studies with 2-Deoxyhexoses. I. Mechanisms of Inhibition of Growth and Fermentation in Baker's Yeast. Biochim Biophys Acta. 1964;86:216-23.
43. Johnson BF. Lysis of yeast cell walls induced by 2-deoxyglucose at their sites of glucan synthesis. J Bacteriol. 1968;95(3):1169-72.

44. McCartney RR, Schmidt MC. Regulation of Snf1 kinase. Activation requires phosphorylation of threonine 210 by an upstream kinase as well as a distinct step mediated by the Snf4 subunit. The Journal of biological chemistry. 2001;276(39):36460-6.
45. Hedbacker K, Carlson M. SNF1/AMPK pathways in yeast. Front Biosci. 2008;13:2408-20.
46. Tu J, Carlson M. REG1 binds to protein phosphatase type 1 and regulates glucose repression in Saccharomyces cerevisiae. EMBO J. 1995;14(23):5939-46.
47. O'Donnell AF, McCartney RR, Chandrashekarappa DG, Zhang BB, Thorner J, Schmidt MC. 2-Deoxyglucose impairs *Saccharomyces cerevisiae* growth by stimulating Snf1-regulated and alpha-arrestin-mediated trafficking of hexose transporters 1 and 3. Mol Cell Biol. 2015;35(6):939-55.
48. Tsujimoto Y, Izawa S, Inoue Y. Cooperative regulation of DOG2, encoding 2-deoxyglucose-6-phosphate phosphatase, by Snf1 kinase and the high-osmolarity glycerol-mitogen-activated protein kinase cascade in stress responses of Saccharomyces cerevisiae. J Bacteriol. 2000;182(18):5121-6.
49. Tatebayashi K, Takekawa M, Saito H. A docking site determining specificity of Pbs2 MAPKK for Ssk2/Ssk22 MAPKKKs in the yeast HOG pathway. EMBO J. 2003;22(14):3624-34.
50. Oh KB, Matsuoka H. Rapid viability assessment of yeast cells using vital staining with 2-NBDG, a fluorescent derivative of glucose. Int J Food Microbiol. 2002;76(1-2):47-53.
51. Stevens T, Esmon B, Schekman R. Early stages in the yeast secretory pathway are required for transport of carboxypeptidase Y to the vacuole. Cell. 1982;30(2):439-48.
52. Kozutsumi Y, Segal M, Normington K, Gething MJ, Sambrook J. The presence of malfolded proteins in the endoplasmic reticulum signals the induction of glucose-regulated proteins. Nature. 1988;332(6163):462-4.
53. Cox JS, Walter P. A novel mechanism for regulating activity of a transcription factor that controls the unfolded protein response. Cell. 1996;87(3):391-404.
54. Teixeira MC, Monteiro P, Jain P, Tenreiro S, Fernandes AR, Mira NP, et al. The YEASTRACT database: a tool for the analysis of transcription regulatory associations in Saccharomyces cerevisiae. Nucleic acids research. 2006;34(Database issue):D446-51.
55. Levin DE. Regulation of cell wall biogenesis in Saccharomyces cerevisiae: the cell wall integrity signaling pathway. Genetics. 2011;189(4):1145-75.
56. Bonilla M, Cunningham KW. Mitogen-activated protein kinase stimulation of Ca(2+) signaling is required for survival of endoplasmic reticulum stress in yeast. Mol Biol Cell. 2003;14(10):4296-305.
57. Krause SA, Xu H, Gray JV. The synthetic genetic network around PKC1 identifies novel modulators and components of protein kinase C signaling in *Saccharomyces cerevisiae*. Eukaryot Cell. 2008;7(11):1880-7.
58. Babour A, Bicknell AA, Tourtellotte J, Niwa M. A surveillance pathway monitors the fitness of the endoplasmic reticulum to control its inheritance. Cell. 2010;142(2):256-69.
59. Chen Y, Feldman DE, Deng C, Brown JA, De Giacomo AF, Gaw AF, et al. Identification of mitogen-activated protein kinase signaling pathways that confer resistance to endoplasmic reticulum stress in Saccharomyces cerevisiae. Mol Cancer Res. 2005;3(12):669-77.
60. Scrimale T, Didone L, de Mesy Bentley KL, Krysan DJ. The unfolded protein response is induced by the cell wall integrity mitogen-activated protein kinase signaling cascade and is required for cell wall integrity in Saccharomyces cerevisiae. Mol Biol Cell. 2009;20(1):164-75.
61. Shackelford DB, Shaw RJ. The LKB1-AMPK pathway: metabolism and growth control in tumour suppression. Nat Rev Cancer. 2009;9(8):563-75.
62. Treitel MA, Kuchin S, Carlson M. Snf1 protein kinase regulates phosphorylation of the Mig1 repressor in Saccharomyces cerevisiae. Mol Cell Biol. 1998;18(11):6273-80.
63. Ferrer-Dalmau J, Randez-Gil F, Marquina M, Prieto JA, Casamayor A. Protein kinase Snf1 is involved in the proper regulation of the unfolded protein response in Saccharomyces cerevisiae. Biochem J. 2015;468(1):33-47.
64. Mizuno T, Masuda Y, Irie K. The Saccharomyces cerevisiae AMPK, Snf1, Negatively Regulates the Hog1 MAPK Pathway in ER Stress Response. PLoS Genet. 2015;11(9):e1005491.
65. Becuwe M, Leon S. Integrated control of transporter endocytosis and recycling by the arrestin-related protein Rod1 and the ubiquitin ligase Rsp5. eLife. 2014;3:03307.

66. McDermott JR, Rosen BP, Liu Z. Jen1p: a high affinity selenite transporter in yeast. Mol Biol Cell. 2010;21(22):3934-41.
67. Bork P, Sander C, Valencia A. An ATPase domain common to prokaryotic cell cycle proteins, sugar kinases, actin, and hsp70 heat shock proteins. Proc Natl Acad Sci U S A. 1992;89(16):7290-4.
68. Chambers JW, Morris MT, Smith KS, Morris JC. Residues in an ATP binding domain influence sugar binding in a trypanosome hexokinase. Biochem Biophys Res Commun. 2008;365(3):420-5.
69. Kuser P, Cupri F, Bleicher L, Polikarpov I. Crystal structure of yeast hexokinase PI in complex with glucose: A classical "induced fit" example revised. Proteins. 2008;72(2):731-40.
70. Aleshin AE, Kirby C, Liu X, Bourenkov GP, Bartunik HD, Fromm HJ, et al. Crystal structures of mutant monomeric hexokinase I reveal multiple ADP binding sites and conformational changes relevant to allosteric regulation. J Mol Biol. 2000;296(4):1001-15.
71. Carlson M, Osmond BC, Neigeborn L, Botstein D. A suppressor of SNF1 mutations causes constitutive high-level invertase synthesis in yeast. Genetics. 1984;107(1):19-32.
72. Trumbly RJ. Isolation of Saccharomyces cerevisiae mutants constitutive for invertase synthesis. J Bacteriol. 1986;166(3):1123-7.
73. Vallier LG, Carlson M. Synergistic release from glucose repression by mig1 and ssn mutations in *Saccharomyces cerevisiae*. Genetics. 1994;137(1):49-54.
74. Guldal CG, Broach J. Assay for adhesion and agar invasion in S. cerevisiae. J Vis Exp. 2006(1):e64.
75. Rothstein RJ, Sherman F. Genes affecting the expression of cytochrome c in yeast: genetic mapping and genetic interactions. Genetics. 1980;94(4):871-89.
76. Teunissen AW, van den Berg JA, Steensma HY. Transcriptional regulation of flocculation genes in Saccharomyces cerevisiae. Yeast. 1995;11(5):435-46.
77. Kuznetsova E, Proudfoot M, Gonzalez CF, Brown G, Omelchenko MV, Borozan I, et al. Genome-wide analysis of substrate specificities of the Escherichia coli haloacid dehalogenase-like phosphatase family. J Biol Chem. 2006;281(47):36149-61.
78. Altschul SF, Madden TL, Schaffer AA, Zhang J, Zhang Z, Miller W, et al. Gapped BLAST and PSI-BLAST: a new generation of protein database search programs. Nucleic acids research. 1997;25(17):3389-402.
79. Preumont A, Rzem R, Vertommen D, Van Schaftingen E. HDHD1, which is often deleted in X-linked ichthyosis, encodes a pseudouridine-5'-phosphatase. Biochem J. 2010;431(2):237-44.
80. Maliekal P, Vertommen D, Delpierre G, Van Schaftingen E. Identification of the sequence encoding N-acetylneuraminate-9-phosphate phosphatase. Glycobiology. 2006;16(2):165-72.
81. Seifried A, Schultz J, Gohla A. Human HAD phosphatases: structure, mechanism, and roles in health and disease. FEBS J. 2013;280(2):549-71.
82. Burroughs AM, Allen KN, Dunaway-Mariano D, Aravind L. Evolutionary genomics of the HAD superfamily: understanding the structural adaptations and catalytic diversity in a superfamily of phosphoesterases and allied enzymes. J Mol Biol. 2006;361(5):1003-34.
83. Cramer FB, Woodward GE. 2-Desoxy-D-glucose as an antagonist of glucose in yeast fermentation. Journal of the Franklin Institute. 1952;253(4):354-60.
84. Woodward GE, Cramer FB, Hudson MT. Carbohydrate analogs as antagonists of glucose in carbohydrate metabolism of yeast. Journal of the Franklin Institute. 1953;256(6):577-87.
85. Woodward GE, Hudson MT. The effect of 2-desoxy-D-glucose on glycolysis and respiration of tumor and normal tissues. Cancer Res. 1954;14(8):599-605.
86. Woodward GE. 2-desoxy-d-glucose as an inhibitor in the aerobic glucose metabolism of yeast. Journal of the Franklin Institute. 1952;254(6):553-5.
87. Kang HT, Hwang ES. 2-Deoxyglucose: an anticancer and antiviral therapeutic, but not any more a low glucose mimetic. Life Sci. 2006;78(12):1392-9.
88. Travers KJ, Patil CK, Wodicka L, Lockhart DJ, Weissman JS, Walter P. Functional and genomic analyses reveal an essential coordination between the unfolded protein response and ER-associated degradation. Cell. 2000;101(3):249-58.
89. Kratky Z, Biely P, Bauer S. Mechanism of 2-deoxy-D-glucose inhibition of cell-wall polysaccharide and glycoprotein biosyntheses in Saccharomyces cerevisiae. Eur J Biochem. 1975;54(2):459-67.

90. Datema R, Schwarz RT. Formation of 2-deoxyglucose-containing lipid-linked oligosaccharides. Interference with glycosylation of glycoproteins. Eur J Biochem. 1978;90(3):505-16.
91. Biely P, Kratky Z, Kovarik J, Bauer S. Effect of 2-deoxyglucose on cell wall formation in Saccharomyces cerevisiae and its relation to cell growth inhibition. J Bacteriol. 1971;107(1):121-9.
92. Utsugi T, Minemura M, Hirata A, Abe M, Watanabe D, Ohya Y. Movement of yeast 1,3-beta-glucan synthase is essential for uniform cell wall synthesis. Genes Cells. 2002;7(1):1-9.
93. Schmidt MF, Schwarz RT, Scholtissek C. Nucleoside-diphosphate derivatives of 2-deoxy-D-glucose in animal cells. Eur J Biochem. 1974;49(1):237-47.
94. Xi H, Kurtoglu M, Lampidis TJ. The wonders of 2-deoxy-D-glucose. IUBMB Life. 2014;66(2):110-21.
95. Biely P, Farkas V, Bauer S. Incorporation of 2-deoxy-D-glucose into glycogen. Biochim Biophys Acta. 1968;158(3):487-8.
96. Lehle L, Schwarz RT. Formation of dolichol monophosphate 2-deoxy-D-glucose and its interference with the glycosylation of mannoproteins in yeast. Eur J Biochem. 1976;67(1):239-45.
97. Steiner S, Lester RL. Studies on the diversity of inositol-containing yeast phospholipids: incorporation of 2-deoxyglucose into lipid. J Bacteriol. 1972;109(1):81-8.
98. Rodriguez A, De La Cera T, Herrero P, Moreno F. The hexokinase 2 protein regulates the expression of the GLK1, HXK1 and HXK2 genes of Saccharomyces cerevisiae. Biochem J. 2001;355(Pt 3):625-31.
99. Gancedo JM. The early steps of glucose signalling in yeast. FEMS Microbiol Rev. 2008;32(4):673-704.
100. Kuo SC, Lampen JO. Inhibition by 2-deoxy-D-glucose of synthesis of glycoprotein enzymes by protoplasts of Saccharomyces: relation to inhibition of sugar uptake and metabolism. J Bacteriol. 1972;111(2):419-29.
101. Gounalaki N, Tzamarias D, Vlassi M. Identification of residues in the TPR domain of Ssn6 responsible for interaction with the Tup1 protein. FEBS Lett. 2000;473(1):37-41.
102. Maqani N, Fine RD, Shahid M, Li M, Enriquez-Hesles E, Smith JS. Spontaneous mutations in CYC8 and MIG1 suppress the short chronological lifespan of budding yeast lacking SNF1/AMPK. Microb Cell. 2018;5(5):233-48.
103. Tzamarias D, Struhl K. Distinct TPR motifs of Cyc8 are involved in recruiting the Cyc8-Tup1 corepressor complex to differentially regulated promoters. Genes Dev. 1995;9(7):821-31.
104. Huh WK, Falvo JV, Gerke LC, Carroll AS, Howson RW, Weissman JS, et al. Global analysis of protein localization in budding yeast. Nature. 2003;425(6959):686-91.
105. Looke M, Kristjuhan K, Kristjuhan A. Extraction of genomic DNA from yeasts for PCR-based applications. Biotechniques. 2011;50(5):325-8.
106. Ma H, Kunes S, Schatz PJ, Botstein D. Plasmid construction by homologous recombination in yeast. Gene. 1987;58(2-3):201-16.
107. Lodi T, Fontanesi F, Guiard B. Co-ordinate regulation of lactate metabolism genes in yeast: the role of the lactate permease gene JEN1. Mol Genet Genomics. 2002;266(5):838-47.
108. Cox J, Mann M. MaxQuant enables high peptide identification rates, individualized p.p.b.-range mass accuracies and proteome-wide protein quantification. Nat Biotechnol. 2008;26(12):1367-72.
109. Cox J, Neuhauser N, Michalski A, Scheltema RA, Olsen JV, Mann M. Andromeda: a peptide search engine integrated into the MaxQuant environment. Journal of proteome research. 2011;10(4):1794-805.
110. Cox J, Hein MY, Luber CA, Paron I, Nagaraj N, Mann M. Accurate proteome-wide label-free quantification by delayed normalization and maximal peptide ratio extraction, termed MaxLFQ. Mol Cell Proteomics. 2014;13(9):2513-26.
111. Hubner NC, Mann M. Extracting gene function from protein-protein interactions using Quantitative BAC InteraCtomics (QUBIC). Methods. 2011;53(4):453-9.
112. Roy A, Dement AD, Cho KH, Kim JH. Assessing glucose uptake through the yeast hexose transporter 1 (Hxt1). PLoS One. 2015;10(3):e0121985.
113. Li H, Durbin R. Fast and accurate short read alignment with Burrows-Wheeler transform. Bioinformatics. 2009;25(14):1754-60.

114. McKenna A, Hanna M, Banks E, Sivachenko A, Cibulskis K, Kernytsky A, et al. The Genome Analysis Toolkit: a MapReduce framework for analyzing next-generation DNA sequencing data. Genome Res. 2010;20(9):1297-303.
115. Robinson JT, Thorvaldsdottir H, Winckler W, Guttman M, Lander ES, Getz G, et al. Integrative genomics viewer. Nat Biotechnol. 2011;29(1):24-6.
116. Ayciriex S, Le Guedard M, Camougrand N, Velours G, Schoene M, Léon S, et al. *YPR139c/LOA1* encodes a novel lysophosphatidic acid acyltransferase associated with lipid droplets and involved in TAG homeostasis. Mol Biol Cell. 2012;23(2):233-46.
117. Orlova M, Barrett L, Kuchin S. Detection of endogenous Snf1 and its activation state: application to Saccharomyces and Candida species. Yeast. 2008;25(10):745-54.
118. Trimble RB, Maley F. Subunit structure of external invertase from Saccharomyces cerevisiae. J Biol Chem. 1977;252(12):4409-12.
119. Brachmann CB, Davies A, Cost GJ, Caputo E, Li J, Hieter P, et al. Designer deletion strains derived from Saccharomyces cerevisiae S288C: a useful set of strains and plasmids for PCR-mediated gene disruption and other applications. Yeast. 1998;14(2):115-32.
120. Jones GM, Stalker J, Humphray S, West A, Cox T, Rogers J, et al. A systematic library for comprehensive overexpression screens in *Saccharomyces cerevisiae*. Nat Methods. 2008;5(3):239-41.
121. Jung US, Sobering AK, Romeo MJ, Levin DE. Regulation of the yeast Rlm1 transcription factor by the Mpk1 cell wall integrity MAP kinase. Mol Microbiol. 2002;46(3):781-9.
122. Turner DL, Weintraub H. Expression of achaete-scute homolog 3 in Xenopus embryos converts ectodermal cells to a neural fate. Genes Dev. 1994;8(12):1434-47.
123. Larkin MA, Blackshields G, Brown NP, Chenna R, McGettigan PA, McWilliam H, et al. Clustal W and Clustal X version 2.0. Bioinformatics. 2007;23(21):2947-8.

Figure Legends

Figure 1. Proteomics analysis of yeast response to 2DG reveals a transcriptional induction of the 2DG6P phosphatases Dog1-Dog2.

(**A**) Volcano-plot representing changes in protein abundance in total protein extracts of wild-type (WT) yeast in response to 2-deoxyglucose (0.2%), obtained by mass spectrometry-based proteomics and analyzed with the MaxQuant software. The x axis corresponds to the $\log_2$ value of the abundance ratio (LFQ: Label-Free Quantification) between 2DG treatment and the negative control. The y axis represents the $-\log_{10}$ of the *p*-value of the statistical t-test for each quantified protein (n=3 independent biological replicates). Line: threshold with a False Discovery Rate of 0.01. (**B**) Western blot on total protein extracts of yeast cells expressing endogenously tagged Dog1-GFP or Dog2-GFP, before and after 2DG addition for the indicated time, using an anti-GFP antibody. A longer exposure is displayed for Dog1-GFP cells to highlight the higher abundance of Dog1 after 2DG addition. Rsp5, whose levels did not change upon 2DG addition in all of our experiments, is used as a loading control. (**C**) Beta-galactosidase assays of wild-type yeast cells expressing *LacZ* under the control of the p*DOG1* or p*DOG2* promoters, before and after 2DG treatments for 3 hours (± SEM, *n*=3). (**D**) Serial dilutions of cultures from the indicated strains were spotted onto SD plates containing no DG or 0.05% 2DG, and grown for 3 days at 30°C. (**E**) Western blot on total extracts of wild-type yeast cells grown overnight in SD medium and treated with 0.2% 2DG or 400mM NaCl for the indicated times. The anti-phospho-p38/Hog1 antibody enables the detection of phosphorylated Hog1 and the anti-p38/Hog1 antibody is used as a control for Hog1 abundance throughout the time course. (**F**) Beta-galactosidase assays of wild-type and *hog1Δ* strains expressing *LacZ* under the control of the p*DOG2* promoter, before and after 2DG treatments for 3 hours. Error bars: SEM (*n*=3). (**G**) Western blot on total protein extracts of WT and *hog1Δ* cells endogenously expressing a Dog2-GFP fusion, before and after 2DG addition for 3h, using an anti-GFP antibody. Total proteins were visualized in gels using a trihalo compound (see *Methods*). (**H**) Relative expression of Dog2-GFP in the same conditions as (**G**) after normalization by total proteins and using WT/untreated as a reference (± SEM, *n*=3).

Figure 2. 2DG leads to Dog2 expression through glycosylation defects that trigger ER stress and the Unfolded Protein Response.

(**A**) Cells expressing endogenously-tagged Loa1-mCherry, used as a control of ER localization (116), were grown overnight in SC medium (exponential phase) and treated with 300µM 2NBDG (see *Methods*) for the indicated times and imaged by fluorescence microscopy. Scale bar: 5 µm. (**B**) WT cells were grown overnight to mid-log phase in SC medium, centrifuged and resuspended in SC-medium

containing mannose (2%) or not, and treated with 0.2% 2DG or 1µg/mL tunicamycin for 4 hours. Total protein extracts were prepared and a western blot on was done using anti-Carboxypeptidase Y (CPY) antibodies. (**C**) Beta-galactosidase assays on WT and *hac1Δ* cells expressing *LacZ* under the control of an UPR-inducible promoter (p*UPRE1*) and treated with 0.2% 2DG or 1µg/mL tunicamycin for 3 hours (± SEM, *n*=3). (**D**) Beta-galactosidase assays on WT cells expressing *LacZ* under the control of the *DOG2* promoter and treated as in (**C**) (± SEM, *n*=3). (**E**) Beta-galactosidase assays on WT and *hac1Δ* cells expressing *LacZ* under the control the *DOG2* promoter, before and after 3h 2DG treatments (± SEM, *n*=3). (**F**) Western blot on total protein extracts of WT and *hac1Δ* cells endogenously expressing a Dog2-GFP fusion, before and after 3h treatment with 2DG or tunicamycin, using an anti-GFP antibody. (**G**) Relative expression of Dog2-GFP in the same conditions as (**F**) after normalization by total proteins and using WT/untreated as a reference (± SEM, *n*=3). (**H**) Serial dilutions of cultures from the indicated strains were spotted onto SC plates (supplemented with 2% mannose when indicated) containing no DG or 0.05% 2DG, and were grown for 3 days at 30°C. (**I**) Serial dilutions of cultures from the indicated strains overexpressing *DOG2* (*pGPD-DOG2)* or not (Ø) were spotted onto SC-Ura plates containing 0, 0.05% or 0.2% 2-deoxyglucose. The plates were scanned after 3 days of incubation at 30°C.

Figure 3. 2DG activates the MAPK-based cell-wall integrity pathway, which is required for 2DG tolerance and additionally contributes to the regulation of Dog2 expression.

(**A**) A WT strain expressing an endogenously-tagged Slt2-GFP construct was grown in SC medium and treated with 2DG (0.2%) or tunicamycin (1 µg/mL). Total protein extracts were prepared at the indicated times and blotted with the following antibodies: anti-p44/42, to reveal activated (phosphorylated) Slt2, and anti-GFP to reveal total levels of Slt2. (**B**) Beta-galactosidase assays on WT and *slt2Δ* cells expressing *LacZ* under the control of an Rlm1-regulated promoter, before and after 3h 2DG (0.2%) or tunicamycin (1 µg/mL) treatments (± SEM, *n*=3). (**C**) *Left*, schematic of the cell wall integrity pathway showing the various actors and their requirement for growth on 2DG (see color code in the inset) based on drop tests showed on the right. *Right*: Serial dilutions of cultures from the indicated deletion strains were spotted onto SD plates containing no DG or 0.05% 2DG, and grown for 3 days at 30°C. (**D**) Beta-galactosidase assays on WT and *slt2Δ* cells expressing *LacZ* under the control the *DOG2* promoter, before and after 3h 2DG treatments (± SEM, *n*=3). (**E**) Western blot on total protein extracts of WT and *slt2Δ* cells expressing an endogenously tagged Dog2-GFP fusion, before and after 3h treatment with 2DG, using an anti-GFP antibody. (**F**) Relative expression of Dog2-GFP in the same conditions as (**F**) after normalization by total proteins and using WT/untreated as a reference (± SEM, *n*=3). (**G**) Serial dilutions of cultures from the indicated strains were spotted onto SC plates (supplemented with 2% mannose when indicated) containing no DG or 0.05% 2DG, and were grown for 3 days at 30°C.

Figure 4. *DOG2*, but not *DOG1*, is controlled by glucose availability through transcriptional repression by Mig1-Mig2 and the kinase Snf1.

(**A**) WT and *snf1Δ* strains, both expressing endogenously tagged Dog1-TAP and Dog2-GFP fusions, were grown overnight in SC medium and then either treated with 0.2% 2DG or switched to an SC-lactate medium for 4 hours. Dog1-TAP was detected with the peroxidase-anti-peroxidase (PAP) complex, Dog2-GFP with anti-GFP antibodies. The anti-Rsp5 antibody was used to control loading. (**B**) Beta-galactosidase activity on WT and *snf1Δ* cells expressing *LacZ* under the control the *DOG1* or the *DOG2* promoter, before and after 3h growth in lactate. The fold-induction after transfer to lactate is indicated for each promoter in each strain (± SEM, *n*=3). (**C**) WT and *snf1Δ* strains, transformed with either a genomic clone containing both *DOG1* and *DOG2* under the control of their own promoter (*pend:DOG*, top panels), or with a vector containing *DOG2* under the control of the strong *GPD* promoter (*pGPD:DOG2*, bottom panels) were grown, serial-diluted and spotted onto SC plates (SC-Leu, top plates, and SC-Ura, bottom plates) with or without 0.2% DG, and grown for 3 days at 30°C. (**D**) Beta-galactosidase assays on WT and the indicated deletion mutants expressing *LacZ* under the control the *DOG2* promoter after overnight growth in SC medium (exponential phase) (± SEM, *n*=3). (**E**) The indicated strains, all expressing an endogenously tagged Dog2-GFP fusion, were grown overnight in SC medium (exponential phase). Total protein extracts were prepared and blotted with anti-GFP antibodies and the anti-Rsp5 antibody was used as a loading control. (**F**) Serial dilutions of cultures of the indicated mutants were spotted on YPD plates containing 0, 0.2% or 0.5% of 2DG. Plates were scanned after 3 days of growth at 30°C.

Figure 5. Most clones that become spontaneously resistant to 2DG show an increased Dog2 expression.

(**A**) 24 clones showing a spontaneous resistance to 0.2% 2DG were isolated. The beta-galactosidase activity of these mutants, due to the expression of the *LacZ* reporter driven by the *DOG2* promoter, was measured after overnight growth in SC medium (exponential phase) (± SEM, *n*=3). For colors, see panels (**B**) and (**D**). (**B**) Serial dilutions of cultures from the indicated deletion strains and resistant clones were spotted onto SC plates containing no DG or 0.2% 2DG, as well as 200 µM selenite or 0.5 µg/mL tunicamycin and grown for 3 days at 30°C. Note that clone #6 grows very slowly even in absence of 2DG. Orange squares: identified *reg1* mutants. (**C**). A WT strain and the 24 resistant clones were grown in SC medium (exponential phase). Total protein extracts were prepared and blotted using antibodies allowing to reveal phosphorylated (activated) Snf1 (anti-phospho-AMPK) or total Snf1 (anti-polyHis tag, because Snf1 contains a stretch of 13 histidine residues that can be used for its detection) (117). The numbers below indicate the ratio of phospho-Snf1 signal over Snf1 signal, relative to the

WT. (**D**) Schematic of the identified mutations within the *REG1* ORF in the indicated mutants as obtained by sequencing. (**E**) The 24 resistant clones were crossed with a WT or an *hxk2*Δ strain of the opposite mating type, and cultures of the haploid resistant clones (see matrix*, left*) or the resulting diploids were spotted onto SC medium with or without 0.2% DG. Green squares: identified *hxk2* mutants.

Figure 6. The 2DG-resistant phenotype of mutants #9 and #10 is caused by a mutation in *CYC8*.

(**A**) Schematic of the domain organization of the Cyc8 protein, showing the Poly(Q) and Poly(QA) repeats as well as the N-terminal TPR repeats. Red: mutation identified by whole genome resequencing of the spontaneous 2DG-resistant mutants #9 and #10. (**B**) A WT strain, the mutant strains #9 and #10 and the *reg1Δ* mutant (positive control) were grown in SC medium (exponential phase). Total protein extracts were prepared and blotted using anti-invertase antibodies (invertase is heavily glycosylated and migrates as a smear (118)). (**C**) WT and mutants #9 and #10 were transformed with low-copy (centromeric) plasmid either empty or containing WT *CYC8* or mutant *cyc8 (Q320*)*, and were spotted on SC-Leu or SC-Leu + 0.2% 2DG medium, and grown for 3 days at 30°C. Middle panel: the control plate was scanned and then washed for 1 min under a constant flow of water, and then scanned again (see Methods). (**D**) Beta-galactosidase activity on WT and mutants #9 and #10 expressing *LacZ* under the control the *DOG2* promoter and transformed with an empty vector or a low-copy vector containing WT *CYC8*, after growth in SC medium (normalized to the value of the WT, ± SEM, *n*=3). (**E**) Western blot on total protein extracts of WT and mutants #9 and #10 cells expressing an endogenously tagged Dog2-GFP fusion and transformed with either an empty plasmid or a low-copy (centromeric) plasmid containing WT *CYC8* after growth in SC medium, using an anti-GFP antibody. (**F**) Relative expression of Dog2-GFP in the same conditions as (**G**) after normalization by total proteins and using the WT control as a reference (± SEM, *n*=3).

Figure 7. The human phosphatase HDHD1 partially rescues the hypersensitivity of a *dog1Δ dog2Δ* mutant to 2DG.

(**A**) Multiple protein sequence alignment of yeast Dog1, Dog2, *Escherichia* coli yniC and the human proteins HDHD1, HDHD4 and PSPH aligned with ClustalX 2.0. The highly conserved catalytic aspartates are displayed in yellow. The six first amino-acids of PSPH were truncated to optimize the N-terminal alignment of its catalytic aspartates with the other phosphatases. (**B**) Serial dilutions of WT and *dog1Δdog2Δ* strains transformed with the indicated plasmids were spotted on SC-Ura medium with or without 0.05% 2DG and were scanned after 3 days of growth at 30°C. (**C**) Serial dilutions of *dog1Δdog2Δ* strains transformed with the indicated plasmids were spotted on SC-Ura medium with or without 0.05% 2DG and were scanned after 3 days of growth at 30°C. (**D**) Total proteins extracts of

dog1Δdog2Δ cells transformed with an empty vector or a vector allowing the overexpression of HDHD4 were blotted with an anti-HDHD4 antibody. (**E**) Serial dilutions of *dog1Δdog2Δ* strains transformed with an empty vector or the indicated vectors allowing the expression of the indicated HDHD1 isoforms were spotted on SC-Ura medium with or without 0.05% 2DG and were scanned after 3 days of growth at 30°C. (**F**) Total protein extracts were prepared from the same strains as in (**E**), and a western blot was revealed with an anti-HDHD1 antibody. The anti-Pgk1 antibody (phosphoglycerate kinase) was used as a loading control.

Figure 8. HDHD1 has a 2DG6P phosphatase activity and its overexpression leads to 2DG resistance in HeLa cells.

(**A**) Serial dilutions of *dog1Δdog2Δ* strains transformed with an empty vector or vectors allowing the expression of a HDHD1 or its predicted catalytic mutant, HDHD1-DD>AA (mutations of the N-terminal catalytic aspartates to alanines) were spotted on SC-Ura medium with or without 0.05% 2DG and were scanned after 3 days of growth at 30°C. (**B**) Total protein extracts were prepared from the same strains as in (**A**), and a western blot was revealed with an anti-HDHD1 antibody. The anti-Pgk1 antibody (phosphoglycerate kinase) was used as a loading control. (**C**) Recombinant, His-tagged HDHD1 and HDHD1-DD>AA were expressed in bacteria and purified for in vitro enzymatic tests. 0.7 µg were loaded on a gel to show homogeneity of the protein purification. (**D**) *In vitro* 2DG6P phosphatase activity of HDHD1 and HDHD1>DDAA as measured by assaying glucose release from 2DG6P. (**E**) Growth of HeLa cells transfected with an empty vector (□) or with a construct allowing the overexpression of HDHD1 (○) over time in the absence (open symbols) or presence (filled symbol) of 5 mM 2DG. The number of cells is normalized to that of the untransformed/untreated cells after 3 days (± SEM, *n*=3). (**F**) Total protein extracts of HeLa cells either untreated (Ø) or treated with 2DG (5 mM) or tunicamycin (5 µg/mL) where blotted with anti-HDHD1 antibodies. Cells transfected with HDHD1 were used as a positive control. The effect of 2DG and Tm on the glycosylation profile of CD147 was used as a control of the efficiency of the treatments.

Figure 9. Working Model.

Glucose phosphorylation triggers the onset of the glucose-repression pathway, by which PP1 inactivates Snf1/AMPK. This leads to the lack of phosphorylation of Mig1/Mig2, which remain in the nucleus to mediate the glucose-repression of genes such as *DOG2*. The deletion of *REG1*, *HXK2*, or *MIG1* and *MIG2,* or a mutation in *CYC8* leads to 2DG resistance, at least in part through an increased expression of *DOG2* which dephosphorylates 2DG-6-P. Instead, the deletion of *SNF1* causes an increased sensitivity to 2DG, which can be rescued by the deletion of *MIG1* and *MIG2* or by Dog2 overexpression. In parallel, 2DG6P causes (i) ER stress and triggers the UPR pathway, which stimulates

1 *DOG2* expression through the transcription factor Hac1, and (ii) the CWI integrity pathway, likely
2 through interference with polysaccharide and cell wall synthesis, which also induces *DOG2* through
3 the transcription factor Rlm1.
4

Supplemental material

Table S1. Proteomic response to 2DG treatment.

See Excel spreadsheet.

Table S2. Single nucleotide variants in clones #9 and #10 as compared to the WT strain, as identified by analysis of whole genome resequencing

Clone	Chrom.	Position	Reference	Mutation	Gene	Mutation in coding region
#9:	chrII	464813	G	A	*CYC8 (YBR112C)*	c.958C>T (p.Gln320X)
	chrXI	570553	C	G	*BET3 (YKR068C)*	c.357G>C (p.Leu119Phe)
	chrXII	969100	C	G	*YLR422W*	c.3204C>G (p.Tyr1068X)
#10	chrII	464813	G	A	*CYC8 (YBR112C)*	c.958C>T (p.Gln320X)
	chrIV	283345	T	A	Intergenic region *GET3-BUG1* (*YDL100C-YDL099W*)	
	chrVIII	303712	T	C	*TRA1 (YHR099W)*	c.952T>C (p.Leu318Leu)
	chrIX	368278	G	C	*PAN1 (YIR006C)*	c.1631C>G (p.Thr544Ser)
	chrXI	570553	C	G	*BET3 (YKR068C)*	c.357G>C (p.Leu119Phe)
	chrXIV	381266	A	C	*DGR1 (YNL130C-A)*	c.126T>G (p.Cys42Trp)
	chrXV	499715	G	A	YOR093C	c.2738C>T (p.Ser913Leu)

Table S3. Yeast strains used in this study.

Name/description	Genotype	Origin/reference	Figures/Panels
BY4741 (WT)	*MATa, ura3Δ0, his3Δ1, leu2Δ0, met15Δ0*	(119)	All
ySL2289 Dog1-GFP	*MATa, ura3Δ0, his3Δ1, leu2Δ0, met15Δ0 DOG1::GFP-HIS3MX6*	This study	1B
ySL2290 Dog2-GFP	*MATa, ura3Δ0, his3Δ1, leu2Δ0, met15Δ0 DOG2::GFP-HIS3MX6*	(104)	1B, 1G, 1H, 4E
ySL2195 *dog1Δ*	*MATa, ura3Δ0, his3Δ1, leu2Δ0, met15Δ0 dog1Δ::KanMX*	Euroscarf deletion collection	1D
ySL2196 *dog2Δ*	*MATa, ura3Δ0, his3Δ1, leu2Δ0, met15Δ0 dog2Δ::KanMX*	Euroscarf deletion collection	1D, 2I
ySL2197 *dog1Δ dog2Δ*	*MATa, ura3Δ0, his3Δ1, leu2Δ0, met15Δ0 dog1Δ-dog2Δ::LEU2MX*	This study	1D, 7B-F, 8A-B
ySL2339 Tdh1-GFP	*MATa, ura3Δ0, his3Δ1, leu2Δ0, met15Δ0 TDH1::GFP-HIS3MX6*	(104)	S1
ySL2340 Stf2-GFP	*MATa, ura3Δ0, his3Δ1, leu2Δ0, met15Δ0 STF2::GFP-HIS3MX6*	(104)	S1

ySL2341 Eno1-GFP	*MATa, ura3Δ0, his3Δ1, leu2Δ0, met15Δ0 ENO1::GFP-HIS3MX6*	(104)	S1
ySL2342 Adh5-GFP	*MATa, ura3Δ0, his3Δ1, leu2Δ0, met15Δ0 ADH5::GFP-HIS3MX6*	(104)	S1
ySL2343 Yro2-GFP	*MATa, ura3Δ0, his3Δ1, leu2Δ0, met15Δ0 YRO2::GFP-HIS3MX6*	(104)	S1
ySL2344 Hor7-GFP	*MATa, ura3Δ0, his3Δ1, leu2Δ0, met15Δ0 HOR7::GFP-HIS3MX6*	(104)	S1
ySL2315 *hog1*Δ	*MATa, ura3Δ0, his3Δ1, leu2Δ0, met15Δ0 hog1Δ::KanMX*	Euroscarf deletion collection	1F, S2
ySL2416 *hog1*Δ Dog2-GFP	*MATa, ura3Δ0, his3Δ1, leu2Δ0, met15Δ0 hog1Δ::KanMX DOG2::GFP-HIS3MX6*	This study	1G, 1H
ySL0052 Loa1-mCherry	*MATa, ura3Δ0, his3Δ1, leu2Δ0, met15Δ0 LOA1::mCherry-KanMX*	(116)	2A
ySL2204 *hac1*Δ	*MATa, ura3Δ0, his3Δ1, leu2Δ0, met15Δ0 hac1Δ::KanMX*	This study	2C, 2E-I, 3G, S3B
ySL2205 *ire1*Δ	*MATa, ura3Δ0, his3Δ1, leu2Δ0, met15Δ0 ire1Δ::KanMX*	Euroscarf deletion collection	2H, 2I
ySL0567 *snf1*Δ	*MATa, ura3Δ0, his3Δ1, leu2Δ0, met15Δ0 snf1Δ::KanMX*	Euroscarf deletion collection	2H, 4B-D
ySL488 Slt2-GFP	*MATa, ura3Δ0, his3Δ1, leu2Δ0, met15Δ0 SLT2::GFP-HIS3MX6*	(104)	3A
ySL1961 *slt2*Δ	*MATa, ura3Δ0, his3Δ1, leu2Δ0, met15Δ0 slt2Δ::KanMX*	Euroscarf deletion collection	3B-G, S4
ySL557 *wsc1*Δ	*MATa, ura3Δ0, his3Δ1, leu2Δ0, met15Δ0 wsc1Δ::KanMX*	Euroscarf deletion collection	3C
ySL2380 *wsc2*Δ	*MATa, ura3Δ0, his3Δ1, leu2Δ0, met15Δ0 wsc2Δ::KanMX*	Euroscarf deletion collection	3C
ySL2379 *wsc3*Δ	*MATa, ura3Δ0, his3Δ1, leu2Δ0, met15Δ0 wsc3Δ::KanMX*	Euroscarf deletion collection	3C
ySL2386 *mtl1*Δ	*MATa, ura3Δ0, his3Δ1, leu2Δ0, met15Δ0 mtl1Δ::KanMX*	Euroscarf deletion collection	3C
ySL2387 *mid2*Δ	*MATa, ura3Δ0, his3Δ1, leu2Δ0, met15Δ0 mid2Δ::KanMX*	Euroscarf deletion collection	3C
ySL481 *ack1*Δ	*MATa, ura3Δ0, his3Δ1, leu2Δ0, met15Δ0 ack1Δ::KanMX*	Euroscarf deletion collection	3C
ySL2384 *rom1*Δ	*MATa, ura3Δ0, his3Δ1, leu2Δ0, met15Δ0 rom1Δ::KanMX*	Euroscarf deletion collection	3C
ySL590 *rom2*Δ	*MATa, ura3Δ0, his3Δ1, leu2Δ0, met15Δ0 rom2Δ::KanMX*	Euroscarf deletion collection	3C
ySL2385 *tus1*Δ	*MATa, ura3Δ0, his3Δ1, leu2Δ0, met15Δ0 tus1Δ::KanMX*	Euroscarf deletion collection	3C
ySL2405 *bck1*Δ	*MATa, ura3Δ0, his3Δ1, leu2Δ0, met15Δ0 bck1Δ::KanMX*	Euroscarf deletion collection	3C, 3G
ySL2382 *mkk1*Δ	*MATa, ura3Δ0, his3Δ1, leu2Δ0, met15Δ0 mkk1Δ::KanMX*	Euroscarf deletion collection	3C
ySL2383 *mkk2*Δ	*MATa, ura3Δ0, his3Δ1, leu2Δ0, met15Δ0 mkk2Δ::KanMX*	Euroscarf deletion collection	3C
ySL2381 *rlm1*Δ	*MATa, ura3Δ0, his3Δ1, leu2Δ0, met15Δ0 rlm1Δ::KanMX*	Euroscarf deletion collection	3C

ySL2297 Dog1-TAP Dog2-GFP	*MATa, ura3Δ0, his3Δ1, leu2Δ0, met15Δ0 DOG1::TAP-KanMX, DOG2::GFP-HIS3MX6*	This study	4A
ySL2298 Dog1-TAP Dog2-GFP *snf1*Δ	*MATa, ura3Δ0, his3Δ1, leu2Δ0, met15Δ0 DOG1::TAP-KanMX, DOG2::GFP-HIS3MX6, snf1Δ::hphNT1*	This study	4A
ySL2292 Dog2-GFP *mig1*Δ	*MATa, ura3Δ0, his3Δ1, leu2Δ0, met15Δ0 DOG2::GFP-HIS3MX6, mig1Δ::KanMX*	This study	4E
ySL2293 Dog2-GFP *mig2*Δ	*MATa, ura3Δ0, his3Δ1, leu2Δ0, met15Δ0 DOG2::GFP-HIS3MX6, mig2Δ::KanMX*	This study	4E
ySL2294 Dog2-GFP *mig1*Δ *mig2*Δ	*MATa, ura3Δ0, his3Δ1, leu2Δ0, met15Δ0 DOG2::GFP-HIS3MX6, mig1Δ::LEU2MX, mig2Δ::KanMX*	This study	4E
ySL2295 Dog2-GFP *hxk2*Δ	*MATa, ura3Δ0, his3Δ1, leu2Δ0, met15Δ0 DOG2::GFP-HIS3MX6, hxk2Δ::KanMX*	This study	4E
ySL2291 Dog2-GFP *reg1*Δ	*MATa, ura3Δ0, his3Δ1, leu2Δ0, met15Δ0 DOG2::GFP-HIS3MX6, reg1Δ::LEU2MX*	This study	4E
ySL2192 *mig1*Δ	*MATa, ura3Δ0, his3Δ1, leu2Δ0, met15Δ0 mig1Δ::KanMX*	Euroscarf deletion collection	4D
ySL2193 *mig2*Δ	*MATa, ura3Δ0, his3Δ1, leu2Δ0, met15Δ0 mig2Δ::KanMX*	Euroscarf deletion collection	4D
ySL2194 *mig1*Δ *mig2*Δ	*MATa, ura3Δ0, his3Δ1, leu2Δ0, met15Δ0 mig1Δ::KanMX, mig2Δ::HIS3MX6*	This study	4D, 4F
ySL2200 *hxk2*Δ	*MATa, ura3Δ0, his3Δ1, leu2Δ0, met15Δ0 hxk2Δ::KanMX*	Euroscarf deletion collection	4D, 4F, 5B
ySL2447 *hxk2*Δ	*MATalpha, ura3Δ0, his3Δ1, leu2Δ0, met15Δ0 hxk2Δ::KanMX*	Euroscarf deletion collection	5E
ySL2199 *reg1*Δ	*MATa, ura3Δ0, his3Δ1, leu2Δ0, met15Δ0 reg1Δ::HIS3MX6*	This study	4D, 4F, 5B, 6B, 6G, 6H
ySL2201 *reg1*Δ *dog1*Δ *dog2*Δ	*MATa, ura3Δ0, his3Δ1, leu2Δ0, met15Δ0 reg1Δ::HIS3MX6, dog1Δ-dog2Δ::LEU2MX*	This study	4F
ySL2202 *hxk2*Δ *dog1*Δ *dog2*Δ	*MATa, ura3Δ0, his3Δ1, leu2Δ0, met15Δ0 hxk2Δ::KanMX, dog1Δ-dog2Δ::LEU2MX*	This study	4F
ySL2203 *mig1*Δ *mig2*Δ *dog1*Δ *dog2*Δ	*MATa, ura3Δ0, his3Δ1, leu2Δ0, met15Δ0 mig1Δ::KanMX, mig2Δ::HIS3MX6, dog1Δ-dog2Δ::LEU2MX*	This study	4F
ySL2317 *mig1*Δ *mig2*Δ *snf1*Δ	*MATa, ura3Δ0, his3Δ1, leu2Δ0, met15Δ0 mig1Δ::KanMX, mig2Δ::HIS3MX6, snf1Δ::NatMX*	This study	4F
ySL2474 mut. #9	Spontaneous mutant arising from BY4741 strain (*MATa, ura3Δ0, his3Δ1, leu2Δ0, met15Δ0*) selected on 0.2% 2DG	This study	5A-C, 6D-G
ySL2475 mut. #10	Spontaneous mutant arising from BY4741 strain (*MATa, ura3Δ0, his3Δ1, leu2Δ0, met15Δ0*) selected on 0.2% 2DG	This study	5A-C, 6D-G
ySL2476 mut. #9-Dog2-GFP	ySL2474 *DOG2::GFP- HIS3MX6*	This study	6F-G
ySL2477 mut. #10-Dog2-GFP	ySL2475 *DOG2::GFP- HIS3MX6*	This study	6F-G

Table S4. Plasmids used in this study.

Name	Description	Origin/reference
pSL209	pGP564: empty vector control for genomic tiling collection, 2µ, *LEU2*	(120)
pSL409	*pDOG1*(1000bp):*lacZ*, 2µ, *URA3* (Yep58-based)	This study
pSL410	*pDOG2*(1000bp):*lacZ*, 2µ, *URA3* (Yep58-based)	This study
pSL405	*pUPRE1*:*lacZ*, 2µ, *URA3* (pGA1695-based)	P. Walter's lab, pJC5 (53)
pSL385	*pCYC(2xRlm1):lacZ* , 2µ, *URA3* (pLGΔ-312-based)	D. Levin's lab, p1434 (121)
pSL412	*pGPD*:*DOG2*, 2µ, *URA3* (pRS426-based)	This study
pSL425	pGP564-based genomic clone YGPM10o10 containing *DOG1* and *DOG2*; 2µ, *LEU2* (genomic tiling collection - chr.VIII:188052-198738)	(120)
pSL438	*pDOG2*(150bp):*lacZ*, 2µ, *URA3* (Yep58-based)	This study
pSL439	*pDOG2*(250bp):*lacZ*, 2µ, *URA3* (Yep58-based)	This study
pSL440	*pDOG2*(350bp):*lacZ*, 2µ, *URA3* (Yep58-based)	This study
pSL441	*pDOG2*(500bp):*lacZ*, 2µ, *URA3* (Yep58-based)	This study
pSL411	*pGPD*:*DOG1*, 2µ, *URA3* (pRS426-based)	This study
pSL413	*pGPD*:*yniC*, 2µ, *URA3* (pRS426-based)	This study
pSL414	*pGPD*:*HDHD1-isoform 1*, 2µ, *URA3* (pRS426-based)	This study
ySL2312	*pGPD*:*HDHD1-isoform 2*, 2µ, *URA3* (pRS426-based)	This study
ySL2313	*pGPD*:*HDHD1-isoform 3*, 2µ, *URA3* (pRS426-based)	This study
ySL2314	*pGPD*:*HDHD1-isoform 4*, 2µ, *URA3* (pRS426-based)	This study
ySL2337	*pGPD*:*HDHD4*, 2µ, *URA3* (pRS426-based)	This study
ySL2336	*pGPD*:*PSPH*, 2µ, *URA3* (pRS426-based)	This study
ySL2335	*pGPD*:*HDHD1-isoform 1-DD>AA*, 2µ, *URA3* (pRS426-based)	This study
pSL422	*pCMV-SPORT6-HDHD1*	Dharmacon
pSL458	*pCS2* (empty vector - expression in mammalian cells)	(122)
pSL431	*pET15b-6His-HDHD1*	E. van Schaftigen (79)
pSL459	*pET15b-6His-HDHD1(DD>AA)*	This study
pSL460	pGP564-based genomic clone YGPM24j02 containing *HXK2*; 2µ, *LEU2* (genomic tiling collection - chr.VII: 23019-35747)	(120)
pSL465	pGP564-based genomic clone YGPM2h11 containing *CYC8*; 2µ, *LEU2* (genomic tiling collection - chr. II: 458726-473023)	(120)
pSL466	*CYC8* (-1000/+300) ; CEN, *LEU2* (pRS415-based)	This study
pSL467	*cyc8*(C^{958}>T) (-1000/+300) ; CEN, *LEU2* (pRS415-based)	This study

Table S5. Antibodies used in this study.

Name	Description	Dilution	Reference/Origin
α GFP	Mouse monoclonal against GFP, clones 7.1 and 13.1	1/5000	11814460001 - Roche
α Rsp5/Nedd4	Rabbit polyclonal antibody against Nedd4	1/5000	ab14592 - Abcam
α ℗p38/℗Hog1	Mouse monoclonal against Tyr182-phosphorylated p38 (E-1)	1/1000	sc166182 - Santa Cruz

α p38/Hog1	Mouse monoclonal against human p38 (D-3)	1/1000	sc165978 - Santa Cruz
α CPY	Rabbit polyclonal against Carboxypeptidase Y (PRC1)	1/2000	ab34636 - Abcam
PAP	Peroxidase-anti-Peroxidase complex	1/5000	P1291 - Sigma Aldrich
α ℗AMPK/℗Snf1	Rabbit polyclonal against Thr172-phosphorylated human AMPKα	1/1000	#2535 - Cell Signaling
α-polyHis tag	Mouse monoclonal antibody used to reveal endogenous Snf1 which contains a stretch of 13 His residues	1/2000	# H1029 - Sigma
α HDHD1	Rabbit polyclonal against human HDHD1. To visualize HDHD1 in lysates of yeast or bacteria overexpressing HDHD1.	1/2000	SAB2700505 - Sigma
α HDHD1	Mouse monoclonal against human HDHD1A (7A2). To visualize HDHD1 in HeLa cell extracts (Panel 7F).	1/1000	NBP2-00487 - Bio-Techne
α HDHD4	Mouse monoclonal anti-HDHD4 (NANP) Antibody (D8). To visualize HDHD4 in lysates of yeast overexpressing HDHD4.	1/5000	sc-374637 - Santa Cruz
α-CD147	Mouse monoclonal anti-CD147 (Clone HIM6)	1/5000	555961–BD Bioscience
α-PGK	Rabbit polyclonal against yeast 3-phosphoglycerate kinase	1/10000	NE130/7S Nordic MUBio
α -Suc2 (invertase)	Rabbit polyclonal against invertase	1/5000	C. Stirling
α Rabbit IgG	Goat secondary antibody against Rabbit IgG	1/5000	A6154 - Sigma Aldrich
α Mouse IgG	Goat secondary antibody against Mouse IgG	1/5000	A5278 - Sigma Aldrich

Supplemental figure legend.

Figure S1. Characterization of other candidates upregulated by 2DG treatment.

(**A**). Western blot on total protein extracts of yeast cells expressing the endogenously GFP-tagged proteins indicated, before and after 2.5h 2DG addition, using an anti-GFP antibody. The anti-Rsp5 antibody is used as a loading control. (**B**) Gene Ontology (GO) analysis of the proteins identified as upregulated in response to 2DG treatment along with their *p*-value and the proteins included in each category.

Figure S2. *DOG1* expression is not regulated by Hog1.

Beta-galactosidase assays of wild-type and *hog1Δ* strains expressing *LacZ* under the control of the p*DOG1* promoter, before and after 2DG treatments for 3 hours. Error bars: SEM (*n*=3).

Figure S3. *DOG1* expression is regulated by the UPR pathway.

(**A**). Beta-galactosidase assays on WT cells expressing *LacZ* under the control of the *DOG1* promoter and treated with 0.2% 2DG or 1µg/mL tunicamycin for 3 hours (± SEM, *n*=3). (**B**). Beta-galactosidase assays on WT and *hac1Δ* cells expressing *LacZ* under the control the *DOG1* promoter, before and after 3h 2DG treatments (± SEM, *n*=3).

Figure S4. Slt2 participates in the regulation of *DOG1* expression.

Beta-galactosidase assays on WT and *slt2Δ* cells expressing *LacZ* under the control the *DOG1* promoter, before and after 3h 2DG treatments (± SEM, *n*=3).

Figure S5. *Cis*-regions involved in the regulation of the *DOG2* promoter by glucose

(**A**). Schematic showing the various constructs generated to study *DOG2* promoter regulation by glucose availability. (**B**). Beta-galactosidase assays on WT cells expressing *LacZ* under the control of the indicated truncated version of the *DOG2* promoter after overnight growth in glucose medium (± SEM, *n*=3).

Figure S6. Multiple protein sequence alignment of Hxk2 orthologues and positions of the mutations identified.

(**A**). Growth test showing that the 2DG sensitivity of the 2DG-resistant clones #1 and #8 can be restored by expression of a multicopy, genomic clone containing *HXK2.* Clone #2 (which displays a mutation in *HXK2*, see **Fig 5**) is used as a positive control. (**B**). List of Hxk2 homologues used for the alignment, as identified using HomoloGene entry #100530 (NCBI). (**C**). The sequences (numbers refer to their GI

numbers) were aligned using ClustalX 2.1 (123) and formatted using BoxShade server (v.3.21). After the alignment, some sequences were truncated in Nt as indicated. The sequence in bold corresponds to that of *S. cerevisiae* Hxk2.

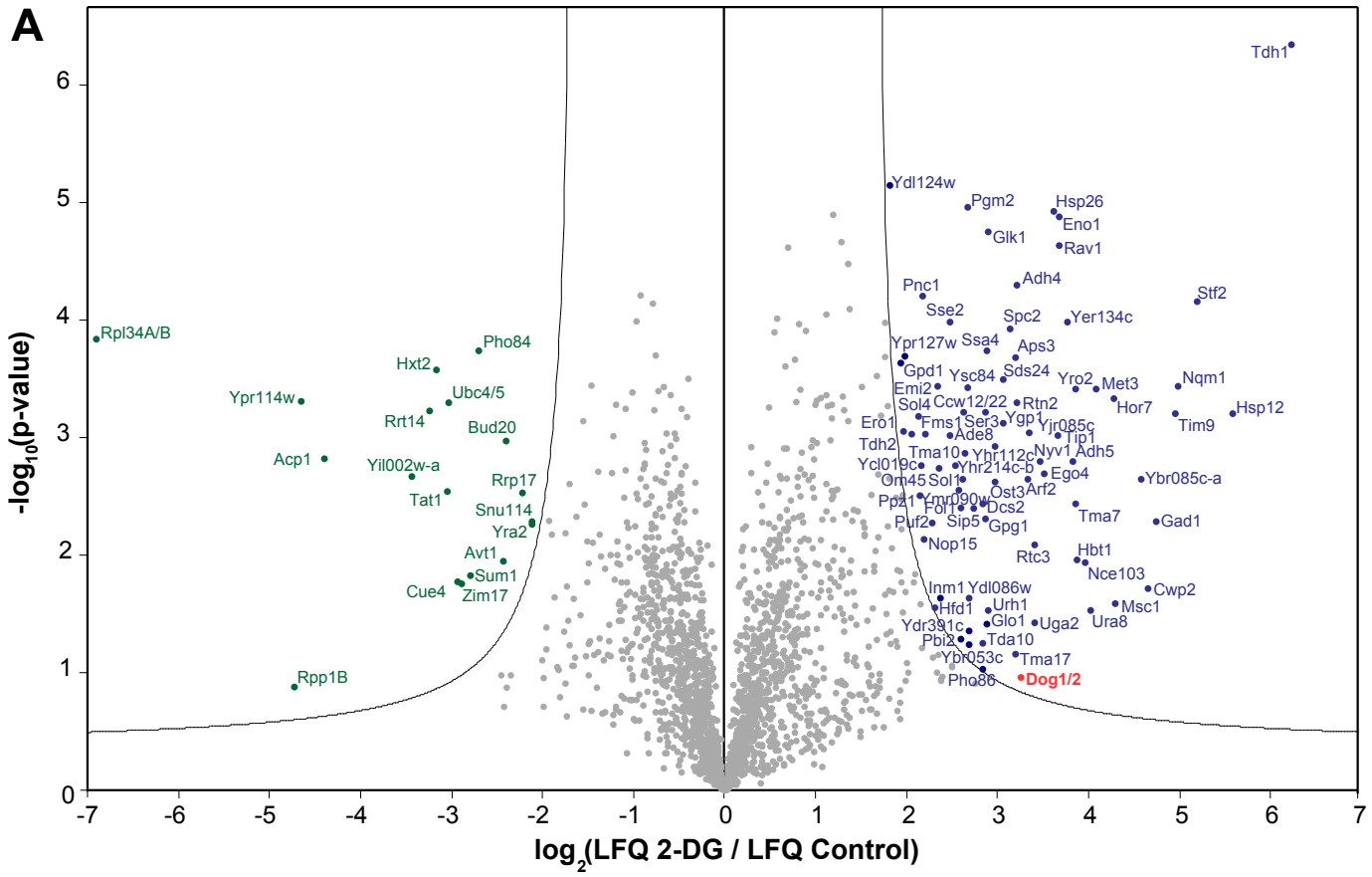

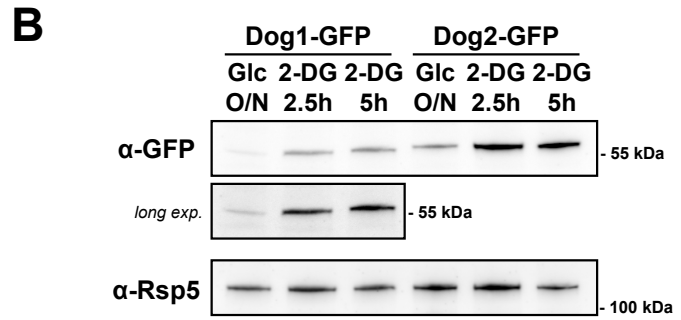

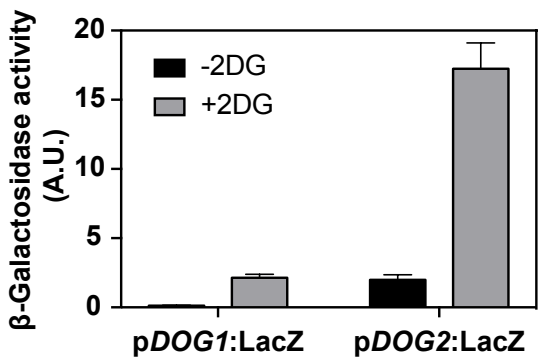

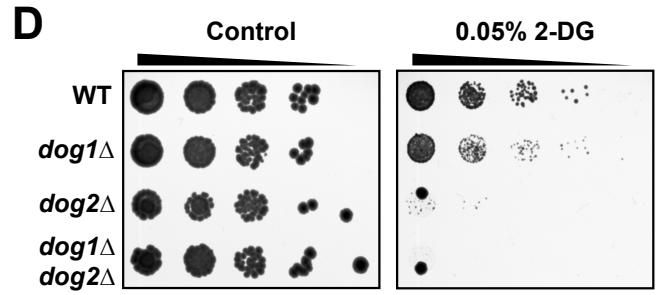

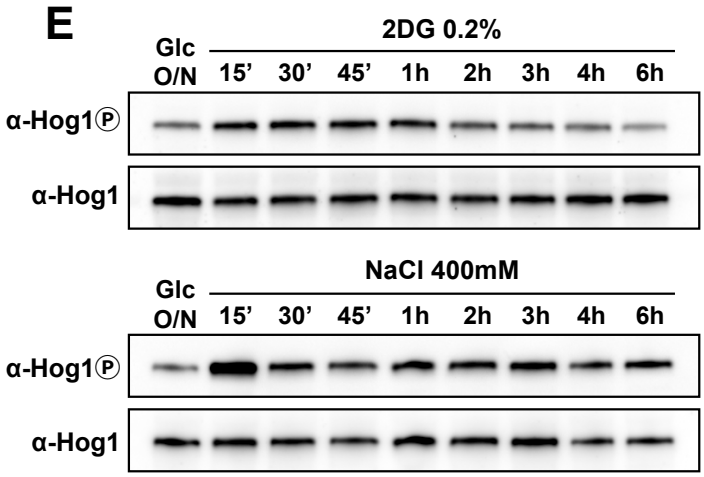

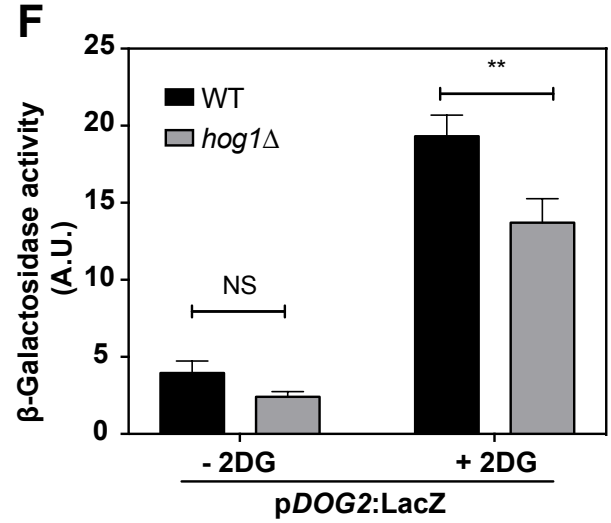

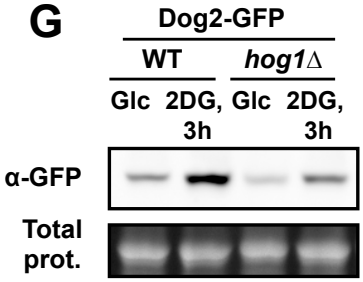

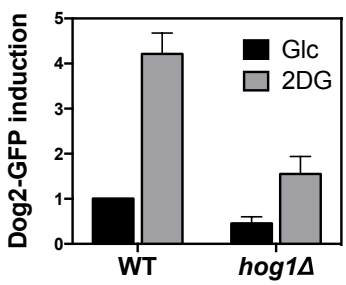

Figure 1; Defenouillère, Verraes et al.

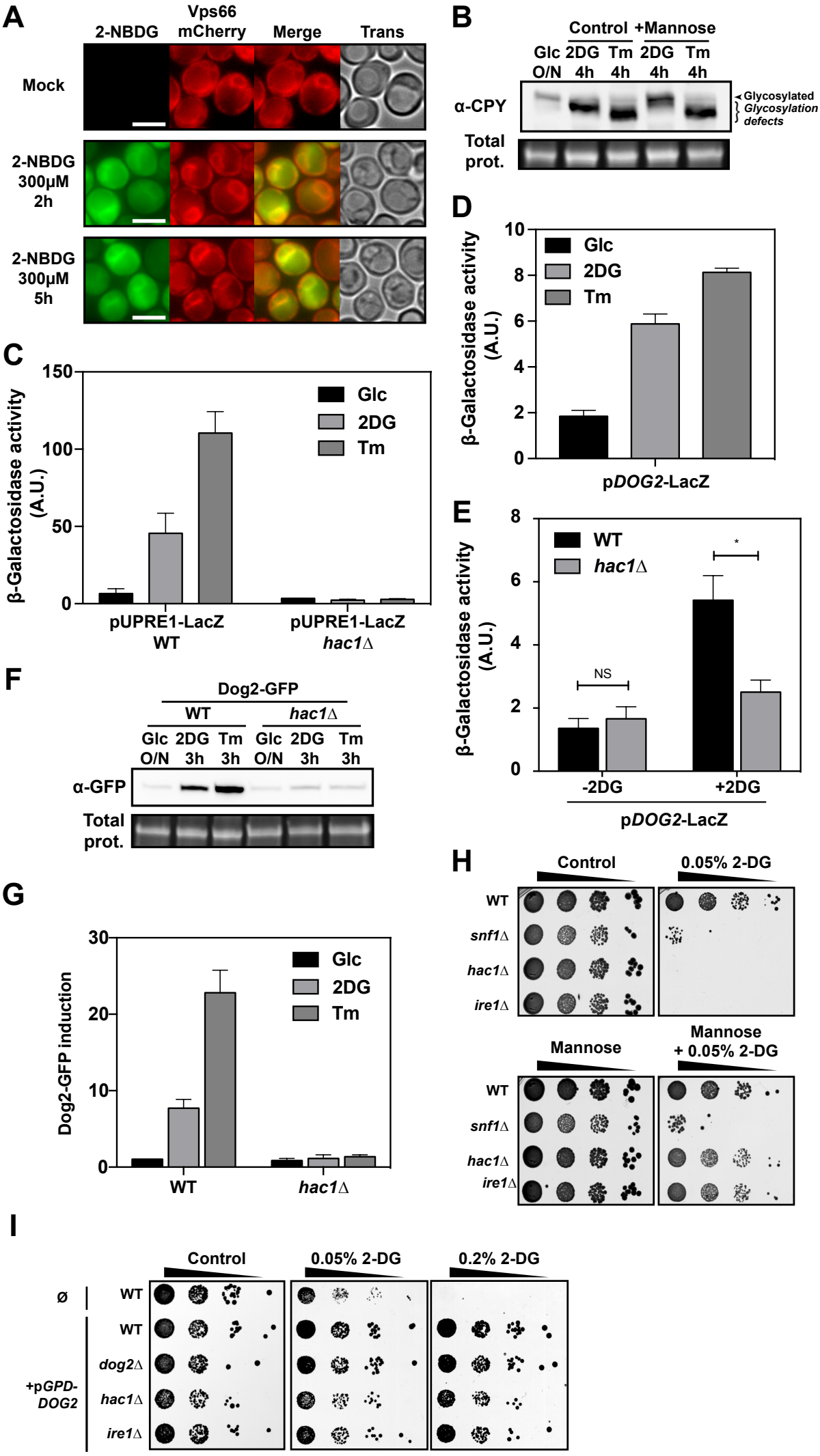

Figure 2; Defenouillère, Verraes et al.

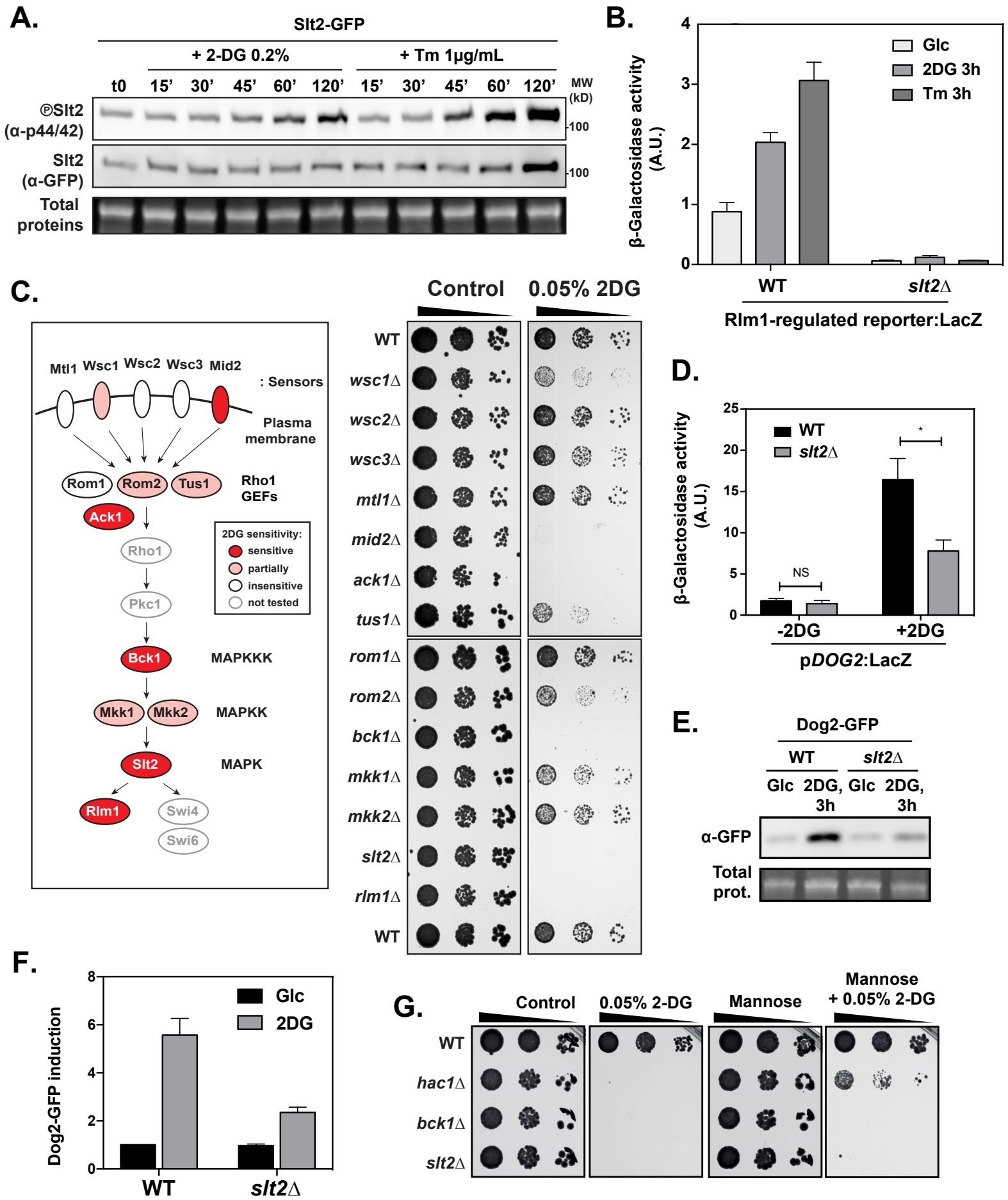

Figure 3; Defenouillère, Verraes et al.

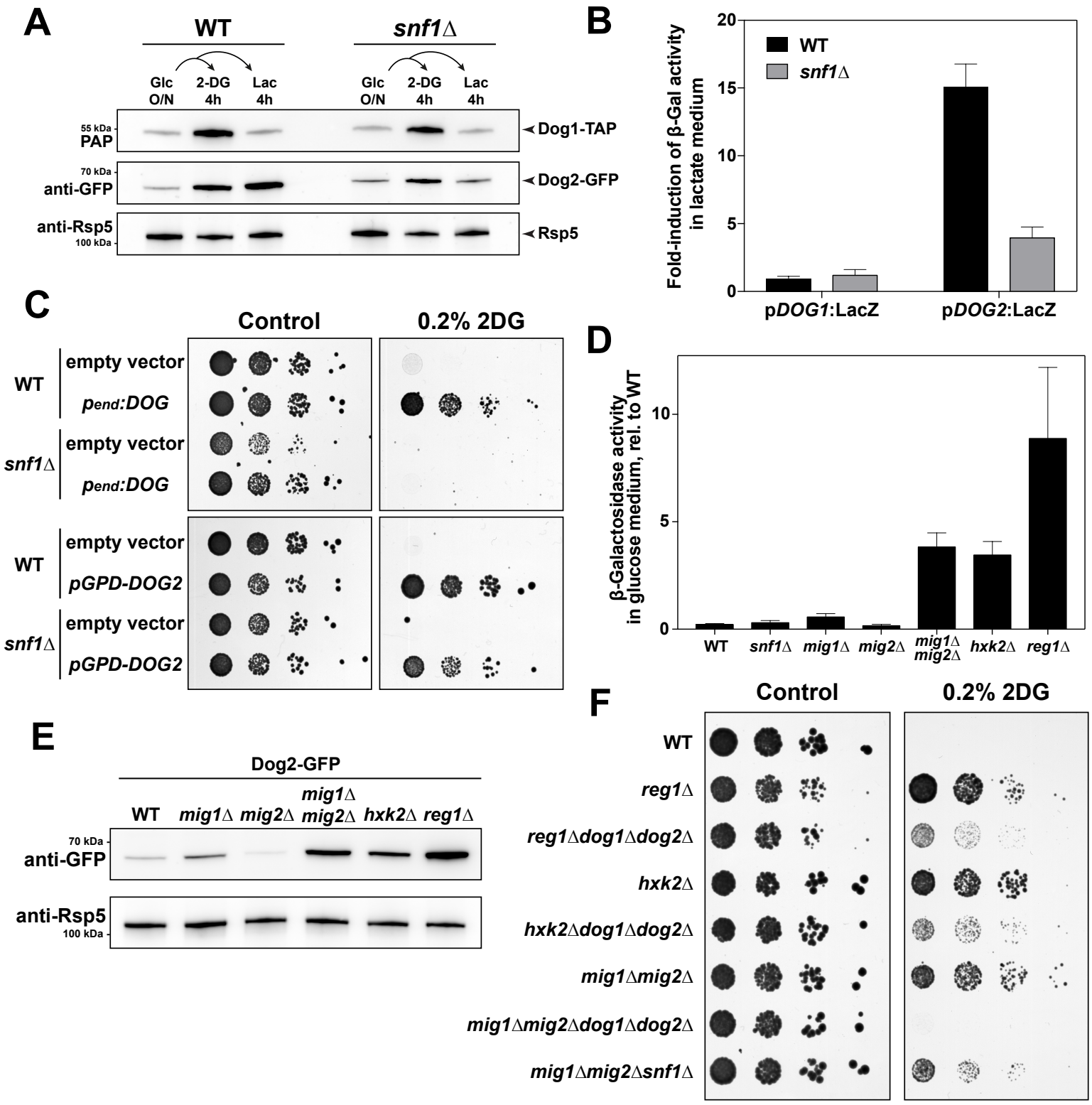

Figure 4; Defenouillère, Verraes et al.

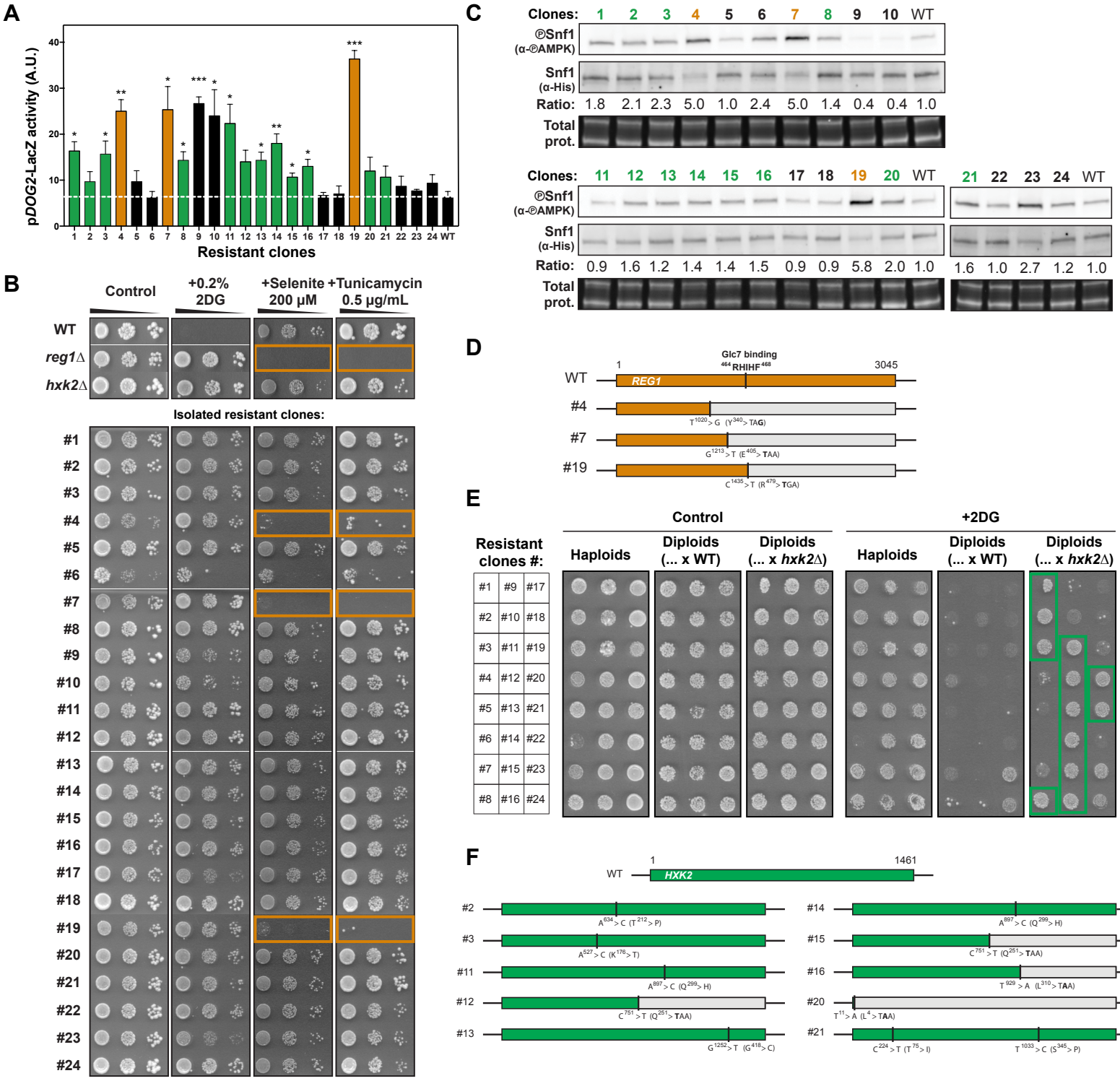

Figure 5; Defenouillère, Verraes et al.

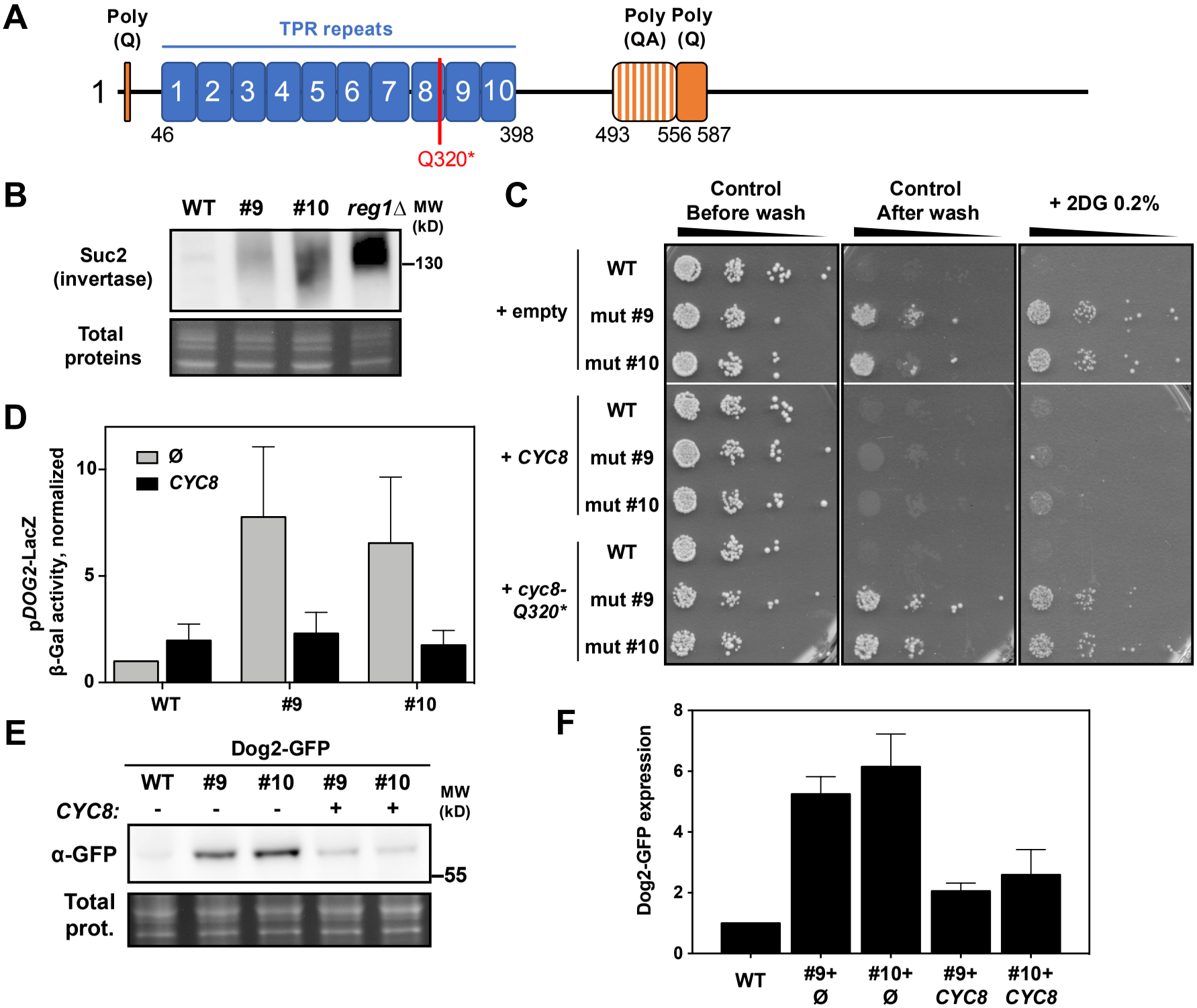

Figure 6; Defenouillère, Verraes et al.

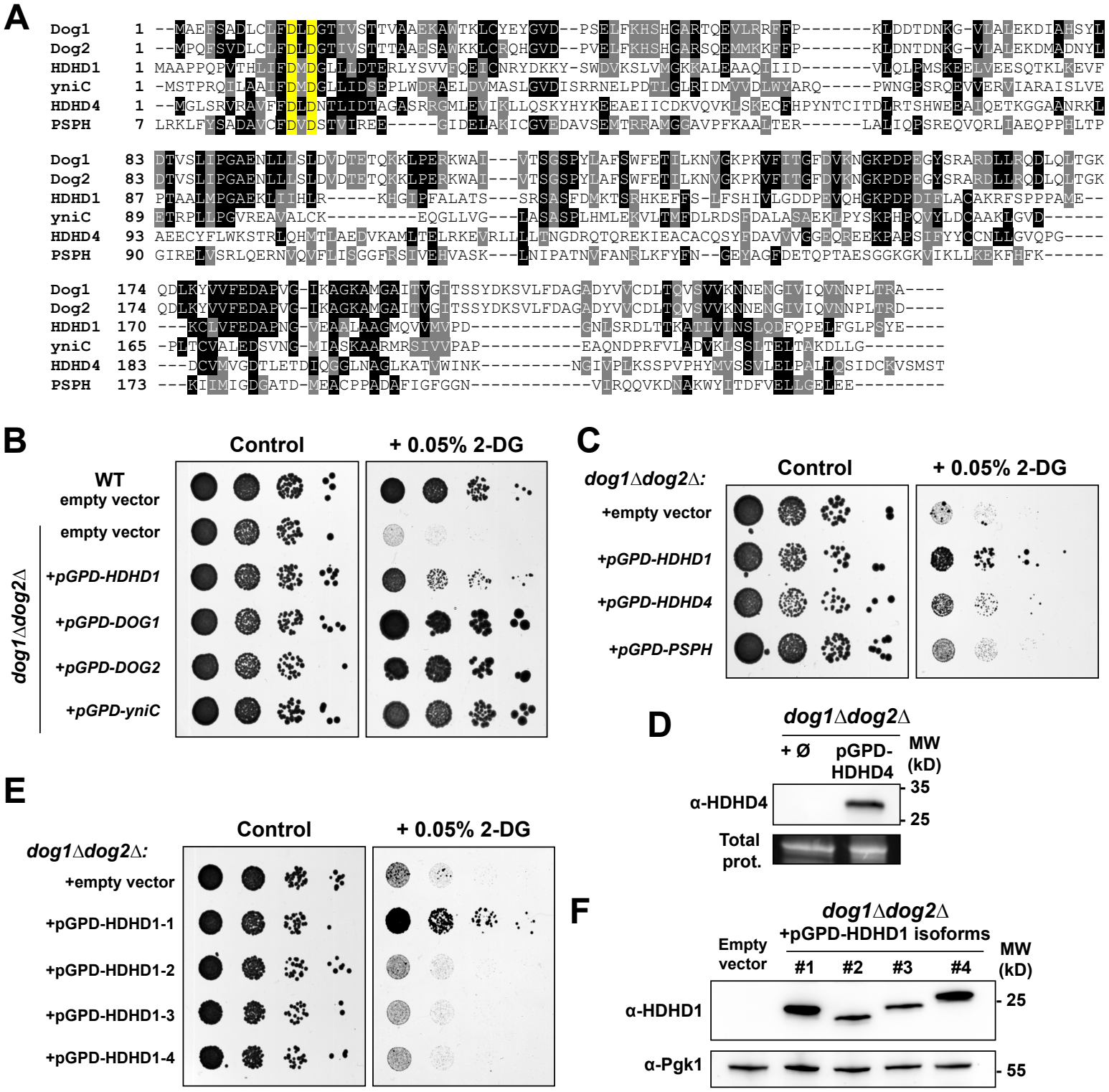

Figure 7; Defenouillère, Verraes et al.

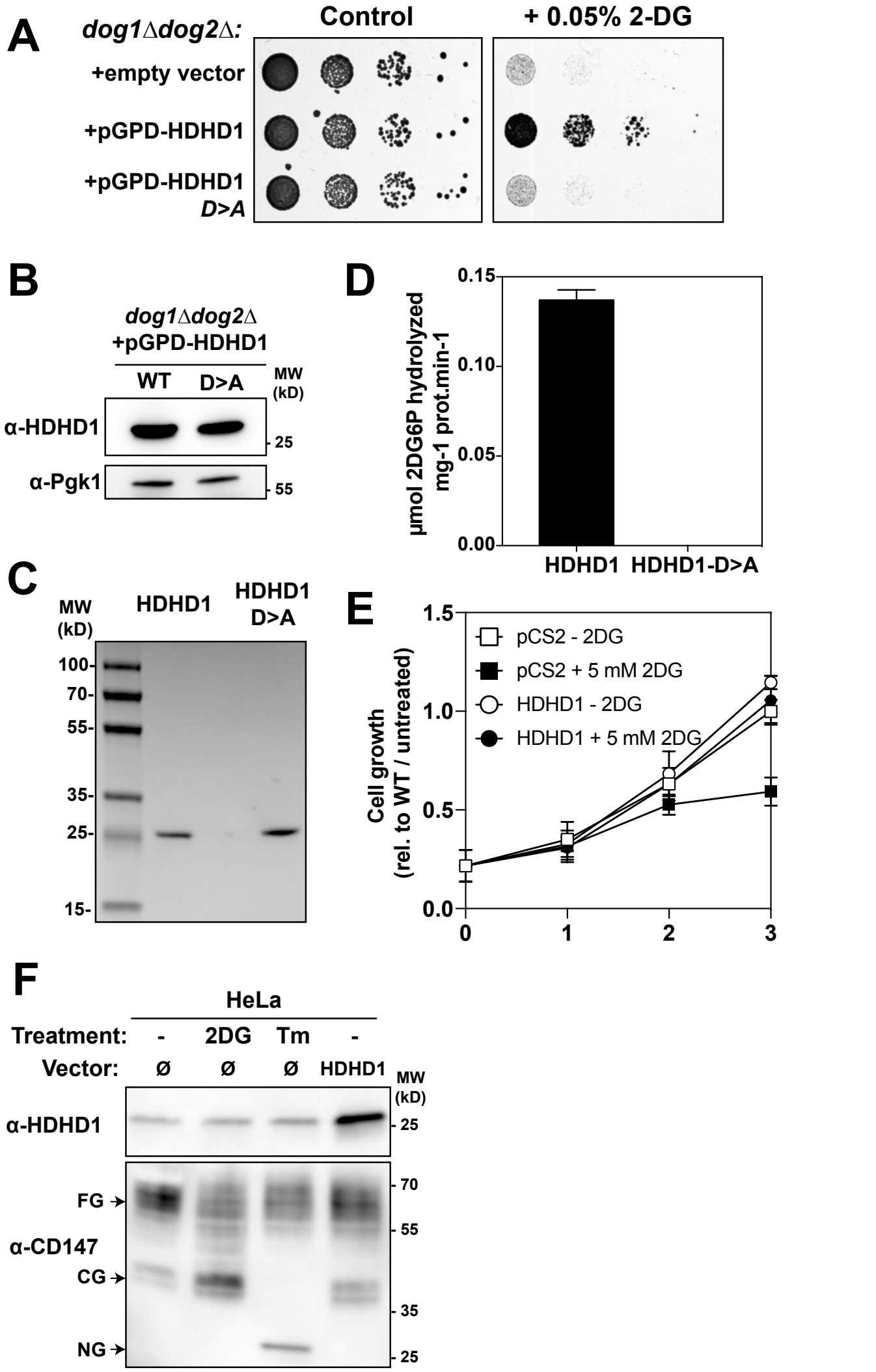

Figure 8; Defenouillère, Verraes et al.

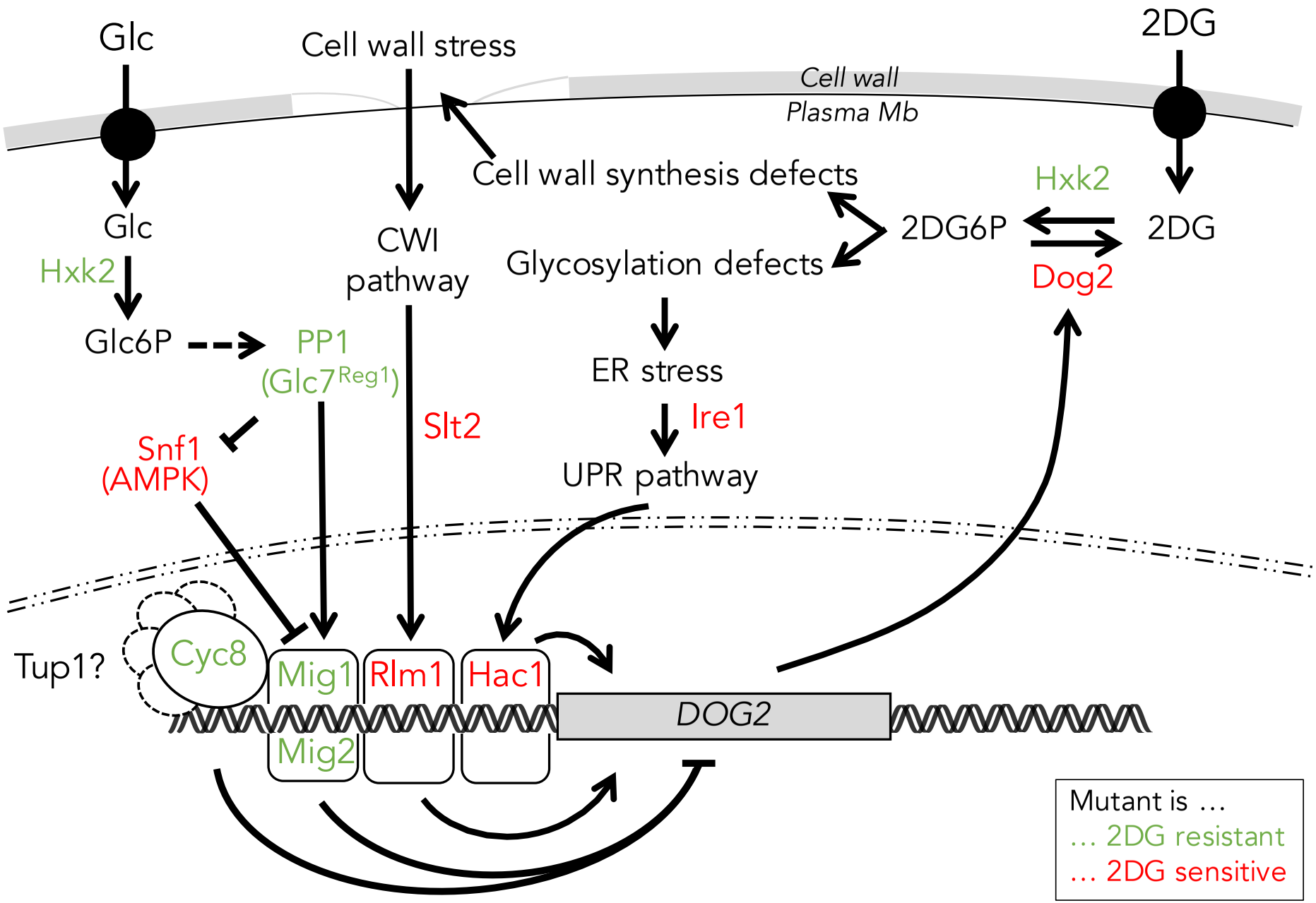

Figure 9; Defenouillère, Verraes et al.

A

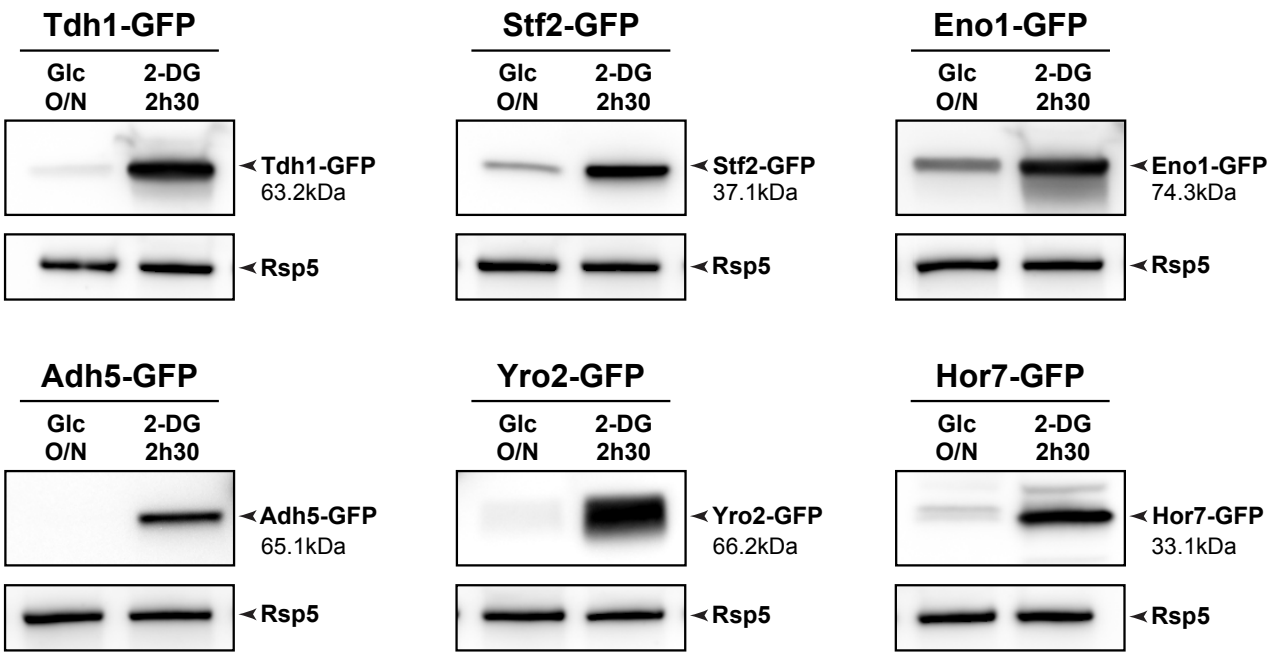

B

GO-term category	p-value	In category from candidates
Glucose metabolic process	**1.519e-07**	Glk1 Dog2 Dog1 Tdh1 Tdh2 Pgm2
Glucose 6-phosphate metabolic process	**5.586e-06**	Glk1 Emi2 Pgm2
Glycolysis	**1.324e-05**	Glk1 Emi2 Eno1 Tdh1 Tdh2
Oxidation-reduction process	**4.798e-05**	Uga2 Adh5 Gpd1 Ydl124w Ser3 Adh4 Tdh1 Tdh2 Ero1 Fms1 Hfd1 Ypr127w
Carbohydrate metabolic process	**8.538e-05**	Glk1 Gpd1 Emi2 Nqm1 Sol4 Pgm2 Sol1
Metabolic process	**0.0002521**	Uga2 Adh5 Gpd1 Urh1 Ser3 Pnc1 Nqm1 Dog2 Dog1 Tdh1 Tdh2 Ymr090w Hfd1 Fol1
Pentose-phosphate shunt	**0.0004683**	Nqm1 Sol4 Sol1
Nicotinate nucleotide salvage	**0.0007527**	Urh1 Pnc1
Cellular response to oxidative stress	**0.0009224**	Uga2 Ydl124w Hsp12 Gad1 Nce103
Gluconeogenesis	**0.001016**	Eno1 Tdh1 Tdh2
Response to stress	**0.001597**	Tip1 Hsp26 Sse2 Gpd1 Ssa4 Hsp12 Hor7
Amino acid catabolic process to alcohol	**0.001854**	Adh5 Adh4
Protein folding	**0.004526**	Hsp26 Sse2 Ssa4 Pho86 Ero1
NADH oxidation	**0.005401**	Adh5 Gpd1

Defenouillère et al., Figure S 1

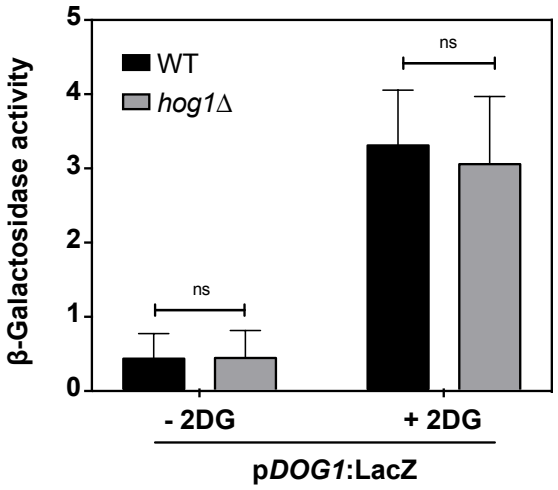

Defenouillère et al., Figure S2

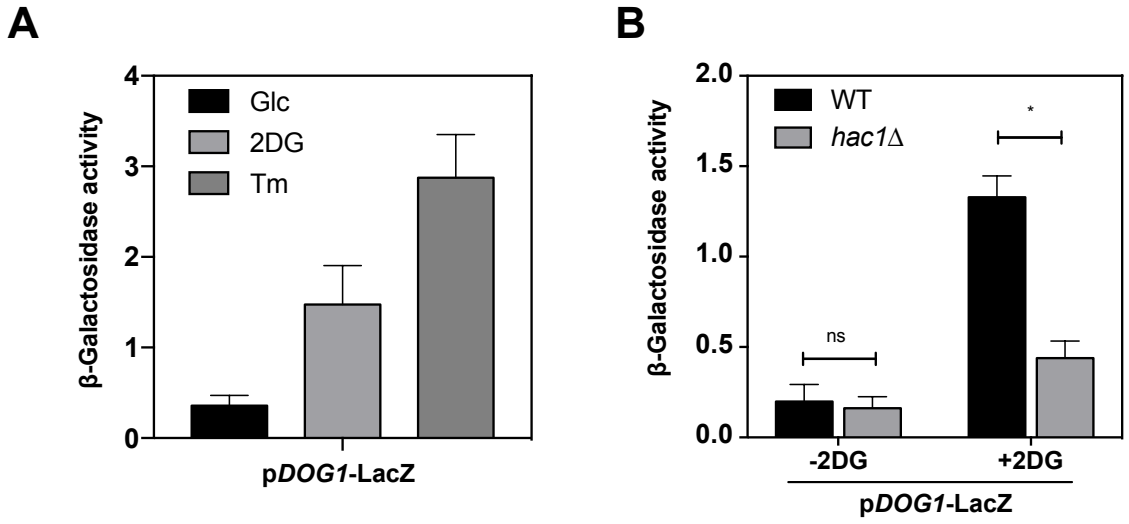

Defenouillère et al., Figure S3

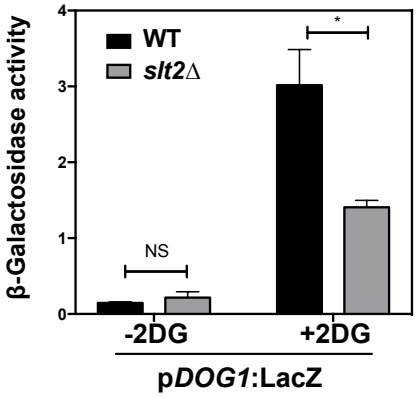

Defenouillère et al., Figure S4

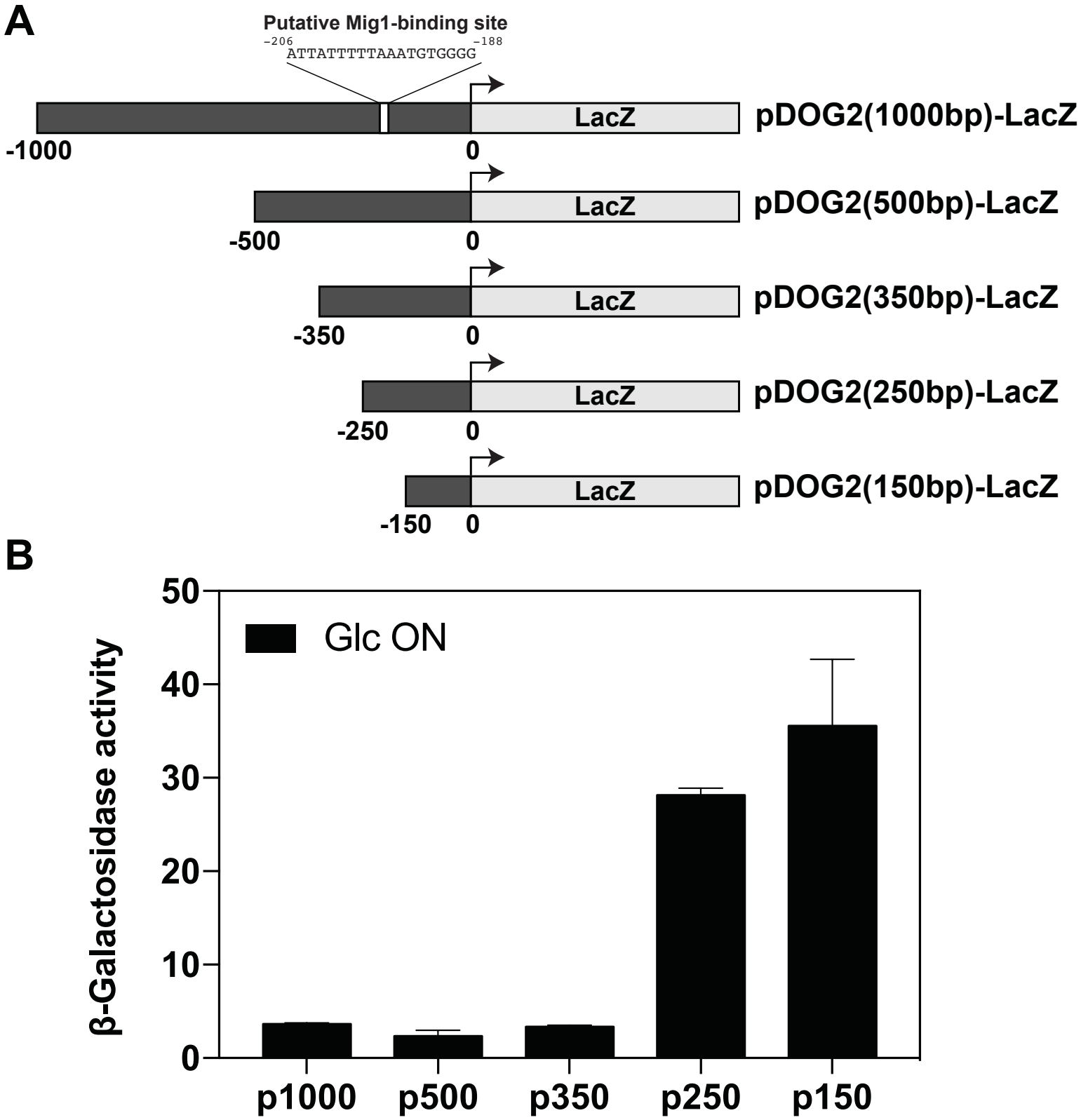

Defenouillère et al., Figure S5

A

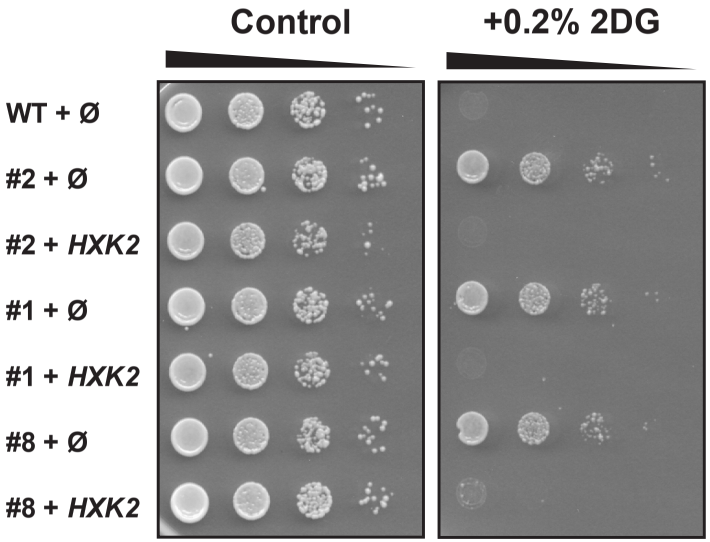

B

GI	Accession	Description	Species
188497754	NP_000179.2	hexokinase-1 isoform HKI	*Homo sapiens*
410043908	XP_001169264.2	hexokinase-1 isoform 9	*Pan troglodytes*
297301245	XP_001110396.2	hexokinase-1-like isoform 6	*Macaca mulatta*
345798984	XP_536376.3	hexokinase-1 isoform X3	*Canis lupus familiaris*
60592784	NP_001012686.1	hexokinase-1	*Bos taurus*
225735584	NP_001139572.1	hexokinase-1 isoform HK1	*Mus musculus*
6981022	NP_036866.1	hexokinase-1	*Rattus norvegicus*
45383904	NP_989432.1	HK1 gene product	*Gallus gallus*
54606886	NP_998417.1	hexokinase-1	*Danio rerio*
45551986	NP_733151.2	Hex-t2	*Drosophila melanogaster*
17864242	NP_524674.1	hexokinase C	*Drosophila melanogaster*
18079297	NP_524848.1	hexokinase A, isoform	*Drosophila melanogaster*
398364415	NP_116711.3	hexokinase 1	*Saccharomyces cerevisiae S288C*
6321184	**NP_011261.1**	**hexokinase 2**	***Saccharomyces cerevisiae S288C***
50307177	XP_453567.1	KLLA0_D11352g	*Kluyveromyces lactis*
45198797	NP_985826.1	AFR279Cp	*Eremothecium gossypii ATCC 10895*
19113860	NP_592948.1	hexokinase 1	*Schizosaccharomyces pombe*
389624569	XP_003709938.1	hexokinase	*Magnaporthe oryzae 70-15*
164427891	NP_965673.2	hexokinase	*Neurospora crassa OR74A*
15224857	NP_179576.1	hexokinase 2	*Arabidopsis thaliana*
15233457	NP_194642.1	hexokinase 1	*Arabidopsis thaliana*
115464965	NP_001056082.1	Os05g0522500	*Oryza sativa Japonica Group*
115439869	NP_001044214.1	Os01g0742500	*Oryza sativa Japonica Group*
156717322	NP_001096201.1	hexokinase-1	*Xenopus tropicalis*

C

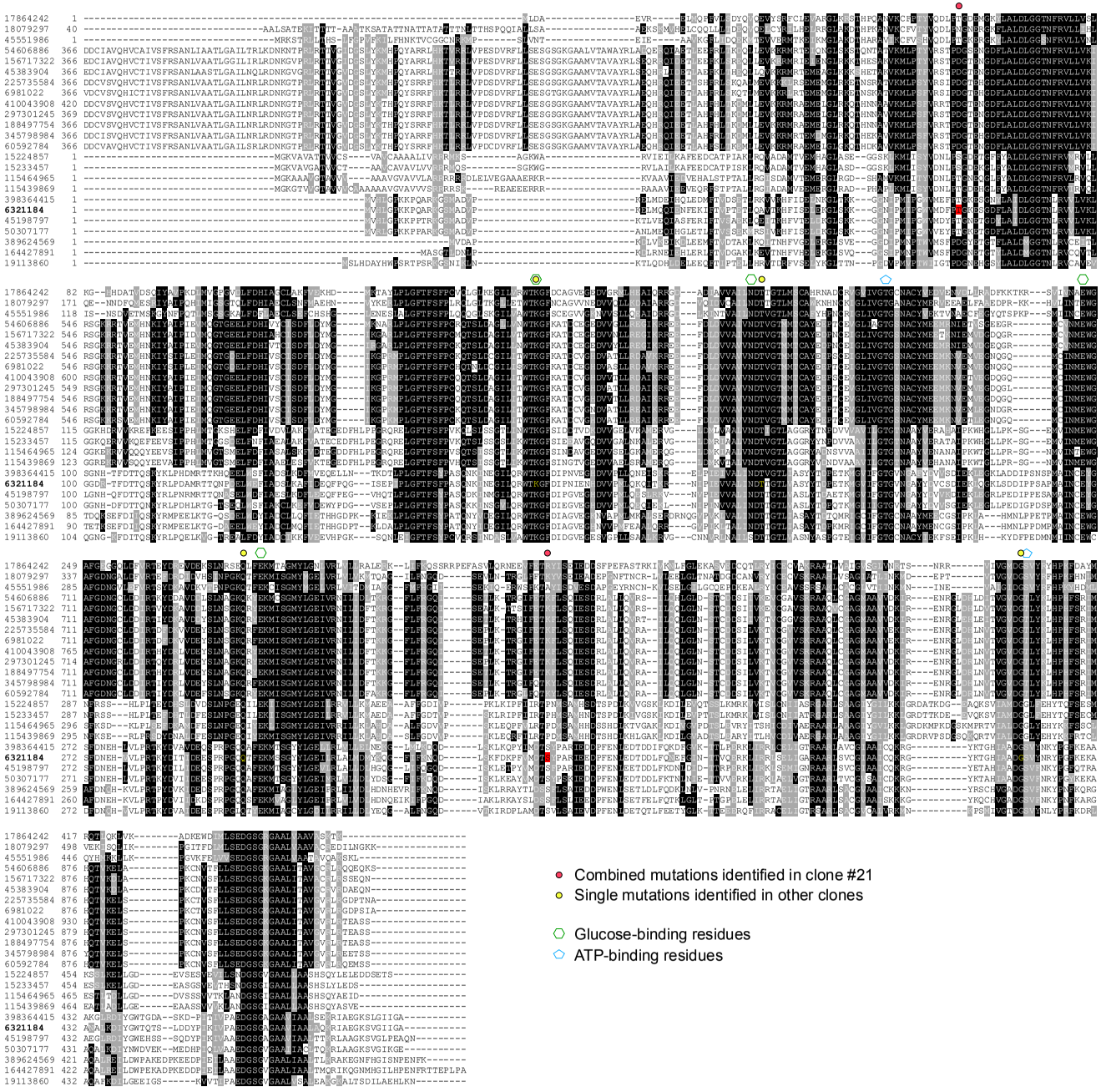

Defenouillère et al., Figure S6